Bioorganic Chemistry 154 (2025) 108046

Contents lists available at ScienceDirect

Bioorganic Chemistry

journal homepage: www.elsevier.com/locate/bioorg

Metabolomic fingerprinting, molecular modelling and experimental bioprospection of *Helianthus annuus* seed cultivars as *Pseudomonas aeruginosa* LasR modulators

Akshay Raghoonanadan, Yamkela Dweba, Christiana E. Aruwa, Saheed Sabiu *

Department of Biotechnology and Food Science, Faculty of Applied Sciences, Durban University of Technology, Durban 4000, KwaZulu-Natal, South Africa

ARTICLE INFO

Keywords:
Helianthus annuus
Metabolome
Quorum sensing
P. aeruginosa
In silico
In vitro
Anti-biofilm

ABSTRACT

The *Pseudomonas aeruginosa* LasR quorum sensing system (QSS) is central to regulating the expression of several pathogenicity factors. Also, while seed- and/or plant-derived products have been investigated as QSS regulators, the impact of *Helianthus annuus* (Pannar sunflower seed cultivars) extracts and metabolites as LasR modulators remain underexplored. Thus, this study focused on the untargeted metabolomic profiling (Liquid Chromatography-Mass Spectrometry), *in vitro* and *in silico* (docking, pharmacokinetics, dynamic simulation) bioprospection of Pannar seed cultivars' extracts and metabolites as LasR modulators. The extracts showed significant QS modulating properties (motility, violacein, biofilm, cell attachment, pyocyanin inhibition) with the PAN 7102 CLP seed cultivar (74.3 %) being the most potent, compared to azithromycin (65 %) and cinnamaldehyde (62 %). Chemometric principal component analysis (PCA) analysis showed distinct metabolite signatures with 52.5 % variance across the six cultivars that was driven by aqueous and ethanolic extracts of PAN 7102, 7160, and 7156 cultivars. The presence of methoxymellein, hydroxytetradecanedioic acid, koninginin G, geoside, pinellic acid and methylpicraquassioside A were reported for the first time. The profiled metabolites were subjected to a 100-ns molecular dynamics simulation following molecular docking. Binding free energy (ΔG_{bind}) calculations revealed obolactone (−48.26 kcal/mol), 1,4-bis(phenylglyoxaloyl)benzene (−45.06 kcal/mol), cyclocanaliculatin (−43.41 kcal/mol), 5-hydroxy-7-methoxy-2-phenylchroman-4-one (−39.18 kcal/mol) and lonchocarpin (−33.78 kcal/mol) as first-time putative leads relative to azithromycin (−32.09 kcal/mol). All lead metabolites also conformed to Lipinski's rule of 5 (Ro5), and their LasR bound complexes were thermodynamically stable and compact given their strong bond interactions. Findings indicate that metabolomic profiling remain key to identifying new compounds from underexplored species. *H. annuus* lead metabolites and extracts may also play key roles as LasR modulators. Further structural modification of the 5 leads could aid their development into novel, oral therapeutics targeting LasR to mitigate resistant *P. aeruginosa* infections.

1. Introduction

Antimicrobial resistance (AMR) remains a global scourge requiring urgent action in form of novel antimicrobials [1]. It is a public health threat ravaging both developed and developing economies [2]. AMR-associated infections cause rise in treatment costs and prolonged hospital stay [3], with billions of Euros spent annually in fighting the scourge [4]. In America, the Centre for Disease Control and Prevention (CDC) also estimated over $18 billion surplus in AMR-linked management costs [3]. Similarly, in 2019, the mortality rate from AMR bacterial infections was approximated to over four million deaths globally, with prediction of ten million deaths per year by 2050, especially in the African and Asian continents [1]. In South Africa, reports of AMR and pandrug-resistant (PDR) infections in patients increased in the past ten years, thus calling for drastic measures to safeguard threats to public health. South Africa has the highest antiretroviral treatment programme and high burden of tuberculosis (TB), with quadrupled resistant infections since 2011 [5]. The first report of colistin resistant genes emergence in infections caused by bacteria constituted a key example of increasing AMR trends in South Africa [6]. As a result, the nation's Departments of Health prioritized studies on drug repurposing, compounding, and bioprospection for novel antibacterial interventive

* Corresponding author.
E-mail addresses: 21925527@dut4life.ac.za (A. Raghoonanadan), 21839429@dut4life.ac.za (Y. Dweba), christianaa@dut.ac.za (C.E. Aruwa), sabius@dut.ac.za (S. Sabiu).

https://doi.org/10.1016/j.bioorg.2024.108046
Received 1 June 2024; Received in revised form 26 November 2024; Accepted 6 December 2024
Available online 10 December 2024

therapies against resistant microorganisms like *Pseudomonas aeruginosa* [7].

Antibiotic resistance and biofilm formation make up part of microbial virulence factors and microbial quorum sensing systems (QSSs) are critical regulators in biofilm development [8]. As such, it has been posited that modulating QSSs could be key to reducing evolutionary pressure in microbial AMR transfer and development [8,9]. In a bid to streamline and fast-track current and future efforts targeting antimicrobials development, the World Health Organization (WHO) classed *Enterococcus faecium*, *Staphylococcus aureus*, *Klebsiella pneumoniae*, *Acinetobacter baumannii*, *P. aeruginosa*, and *Enterobacter* spp. (ESKAPE) as priority pathogens urgently needing new antimicrobials [10]. Of these, *P. aeruginosa* shows the highest mortality rate (above 40 %) and is the most implicated in hospital- and community-acquired infections in immunocompromised patients [11]. This Gram-negative bacterium also shows multi-drug resistance (MDR) to several groups of antibiotics including macrolides, β-lactams, fluoroquinolones, and the last line of defence antibiotics (polymyxins, carbapenems, glycopeptides) [12].

As a versatile, opportunistic pathogen, virulence in *P. aeruginosa* is associated with its central LasR QSS, and it has been demonstrated that use of QS inhibitors (QSIs) interfering with QS mechanisms is a feasible approach to inhibit the formation of bacterial biofilms and other virulence factors for mitigation of pathogenicity in *P. aeruginosa* [13]. In addition, the development of innovative alternative therapies and novel antimicrobials remains imperative as druggable microbial targets evolve relative to the limited number of antibiotics. Likewise, since many currently available antibiotic interventions have been misused and abused, are expensive and come with side effects such as nausea, diarrhoea, bloating and indigestion [14], there is the need to source for natural plant-based products as potential alternative novel antimicrobials. Consequently, plant natural products including seeds' bioprospection has been embraced to provide more effective, safe, natural and affordable treatment options with antimicrobial and QS modulating properties [15,16].

The use of plants as therapeutics in trado-medical practices are well known. A notable therapeutic plant species of importance is the *Helianthus annuus* L. (sunflower, in the family Asteraceae). The *H. annuus* hybrid seeds are an underutilized bioresource in South Africa, and their metabolome are scarcely profiled in metabolomic workflows [16]. The seed cultivars are mostly used in the extraction of sunflower seed oil, baked food products or as food garnishes and snacks [15]. The recorded pharmacological activity range of *H. annuus* sprout and seeds include cardiovascular, antimicrobial, antioxidant, wound healing and anti-inflammatory properties [17]. These activities are attributed to the presence of vitamins, phenolics, flavonoids, unsaturated fatty acids [17,18]. These notable medicinal, nutritional, and culinary benefits have resulted in the growing global popularity of the sunflower species and hybrids. One of such sunflower hybrids is the Pannar seed cultivar which provides exceptional adaptability, stability, oil content and yields, and are bred to be resistant to draught and phytopathogenic fungi [17]. In addition, an earlier study had reported the anti-quorum sensing (AQS) effects of *H. annuus* seed oils derived from Agsun hybrid cultivars. The work also reported the lead metabolite (phylloquinone) responsible for the AQS activity following metabolomic profiling (Gas Chromatography-Mass Spectrophotometry), and computational bioprospection of profiled metabolites [19]. Nevertheless, no study is available on the comparative metabolomic profile and QS modulatory potential of sunflower Pannar (PAN) seed cultivars using *in vitro* and *in silico* methods. In light of the foregoing, there is the need to bridge the knowledge gap in Pannar hybrid seeds metabolite profiles, and the potential use of its extracts and lead molecules in *P. aeruginosa* LasR QSS modulation. Therefore, as an innovative strategy, this study explored the metabolomic fingerprints of extracts (using Ultra-High Performance Liquid Chromatography coupled with Mass Spectrometry analysis) from six underutilized South African hybrid, sunflower seed (Pannar) cultivars (PAN 7158 HO, PAN 7102 CLP, PAN 7156 CLP, PAN 7160 CLP, PAN 7170, PAN 7180 CLP) to enhance their use in QSIs development. Thereafter, seed extracts were subjected to *in vitro* antibacterial and AQS assays, followed by use of extracts' profiled metabolites in computational modelling [molecular docking, molecular dynamics (MD) simulation, pharmacokinetics prediction] to validate their *in silico P. aeruginosa* LasR modulatory capabilities.

2. Materials and methods

2.1. Pannar seed cultivars collection, preprocessing, extraction

Six *Helianthus annuus* seed cultivars (PAN 7102, PAN 7156, PAN 7158, PAN 7160, PAN 7170, PAN 7180) were gotten from the Agricultural Research Council (ARC), Pretoria, South Africa. The cultivars were de-husked, washed with distilled water, and subsequently oven-dried at 40 °C for 24 h. The dehydrated seeds were ground to powdered form using a blender (CaterWize CB-767 model, South Africa), and stored in air-tight containers at 4 °C. Thereafter, about 2 g of each powdered seed cultivar was mixed with 40 mL each solvent [water (A), ethanol (E), hydro-ethanol (EA) and acidified methanol (MF)] in 100 mL conical flasks and the setup was orbitally shaken at 25 °C for 24 h. The extraction mixtures were thereafter filtered using a Whatman No. 1 filter paper, and solvents evaporated from the filtrate by rotary evaporation at 60 rpm and 45 °C. All extracts were re-suspended in 2 % dimethyl sulphoxide (DMSO) and stored at 4 °C prior to further analysis [20]. Using a 0.45 μm filter attached to a syringe, about 0.5 mL of separate extract samples were transferred into glass vials for metabolomic analysis.

2.2. In vitro analyses

The bacterial strains used in *in vitro* assays were the *P. aeruginosa* ATCC 27853, and the quorum sensing bio-monitor strain, *Chromobacterium violaceum* ATCC 12472, which is used to determine extracts or compounds QS modulating potentials by monitoring the expression levels of its violacein virulence factor [21]. *P. aeruginosa* was cultured on Mueller Hinton agar (MHA) plate and incubated at 37 °C for 24 h, and *C. violaceum* on (Luria Bertani) LB agar with incubation at 30 °C for 24 h. Both strains were sub-cultured prior to each test by inoculating a single colony into respective broth media and shaken at 120 rpm at respective temperatures until an optical density (OD) of 0.08 (0.5 McFarland standard equivalent) at 600 nm was reached [22].

2.2.1. Antibacterial susceptibility and microdilution tests

The susceptibility of *P. aeruginosa* cells to extracts was assessed through the agar well diffusion workflow, followed by minimum inhibitory concentration (MIC) determination using the microbroth dilution technique. A standardized bacterial culture (0.5 McFarland) was prepared and 100 μL of the culture was swabbed on the surface of solidified Muller Hinton (MH) agar plates. Then, 6 mm wells were bore into the inoculated plates and 60 μL of plant extracts at different concentrations (400–600 mg/ml) were pipetted into each well and allowed to diffuse into the agar for an hour [23]. Plates were thereafter inverted and incubated (24 h at 37 °C). The same protocol was utilized for the negative control (2 % DMSO), and azithromycin and cinnamaldehyde reference standards served as positive controls. Tests were carried out in triplicate, and the mean diameter of zones of inhibition were recorded in 'mm'.

In the MIC tests, the microbe was assessed for visible growth and MIC determined in the microbroth dilutions using the p-iodonitrotetrazolium chloride (p-INT) growth indicator since plant extracts cause turbidity and precipitation when mixed with growing microbial cultures in media [24]. In determining the MIC, microtiter plate (Sigma-Aldrich, South Africa) wells were first filled with 100 μL of sterile MH broth which were then used to serially (2-fold) dilute extract stock concentrations (100 μL) along each row. Following dilution, 30 μL of standardized bacterial

suspension was pipetted into wells, while two separate wells were used as sterility (MH broth alone) and growth (bacterial suspension alone) controls. This was followed by sealing of plates and incubation for 24 h at 37 °C. Then, 50 μL of a 0.2 mg/ml p-INT violet solution was added to each row and left to incubate for 45 min to 1 h (to allow appreciable development of colour). A decreased/poor colour reaction or development, or observation of a clear solution indicated growth inhibition [25]. The MIC representing the lowest concentration of an antimicrobial agent that inhibits growth was recorded for each extract.

2.2.2. Assessment of extracts anti-quorum sensing activities

The qualitative AQS test was done as described by Chenia [26] with minor modifications. About 50 μL of 0.5 McFarland standard *C. violaceum* culture was spotted in the centre of the plate and swabbed evenly across the surface of the solidified agar. Wells were made and 100 μL crude extracts in the MIC to 1/8 MIC (mg/mL) ranges were transferred into appropriate and respective labelled wells. The same was done for the standards; the QS inhibitor antibiotic (azithromycin) [27], and cinnamaldehyde), as well as the negative control (2 % DMSO). The set up was incubated at 30 °C for 24 h. The plates were thereafter assessed for violacein expression where opaque zones (loss of purple violacein pigment) around wells indicated AQS activity, and clear zones indicated bactericidal activity. Inhibition zones were interpreted as susceptible (≥15 mm), intermediate (11–14 mm) and resistant (≤10 mm) [19].

In the quantitative AQS test, prior to incubation, *C. violaceum* broth culture absorbance ($OD_{485\ nm}$) was checked for violacein production and at $OD_{600\ nm}$ for culture viability. Afterwards the culture was standardized to 0.5 McFarland value of 0.08 at $OD_{600\ nm}$ in sterile LB broth. Then 75 μL of broth and bacterial culture were added into microtiter plate wells, followed by extracts at MIC to 1/8 MIC (mg/mL), and plates were allowed to shake at 30 °C and 120 rpm, for 24 h. Thereafter, absorbance readings were taken ($OD_{485\ nm}$) to measure violacein expression, followed by oven drying of plates. The well contents were re-suspended with 100 μL of 100 % DMSO, allowed to shake in an incubator for 1–2 h at 30 °C and 120 rpm, and an $OD_{485\ nm}$ was used to obtain readings to quantify violacein inhibition and concentration. Tests were done in triplicates and percentage (%) inhibition calculated as below:

$$\%\ \text{inhibition} = (\text{OD control} - \text{OD test})/(\text{OD control}) \times 100$$

Inhibition parameters were ≥50 % (high activity) and 0–49 % (low activity) [28].

2.2.3. Swimming and swarming motility tests

The swimming [agar (0.5 %), sodium chloride (NaCl, 0.5 %, tryptone (1 %)], and swarming (3 % glucose, 0.8 % nutrient broth, 0.5 % agar, w/v) media were prepared. About 2 μL each of standardized *P. aeruginosa* culture (OD of 0.08 at 600 nm) was spotted at the centre of the solidified plates, followed by spotting of extracts (2 μL at varied MIC to 1/8 MIC) directly on top of the previous spot of culture, followed by plates incubation (37 °C, 24 h). The mean diameter of inhibition zones was then recorded (mm) for swimming and swarming plates relative to the negative and positive controls. The experiments were carried out in triplicate [29,30].

2.2.4. Cell attachment and biofilm development inhibition

The modified method described by Famuyide et al. [31] was used. About 50 μL of standardized *P. aeruginosa* culture, 50 μL MH broth, and 50 μL of extracts and standards at MIC to 1/8 MIC were applied to 96-well microtiter plate wells and left to grow for 24 h at 37 °C. Negative (2 % DMSO) and positive (azithromycin) controls were set up in appropriate separate wells. Using crystal violet (CV) formed biofilm biomass was measured. The plates containing the biofilm were carefully rinsed three times in sterile distilled water to dislodge planktonic cells and medium, then oven-dried. Thereafter, plates were incubated in a dark environment for 15 min following addition of modified crystal violet (CV) at 1 % solution. This was followed by a three-time sterile distilled water wash to remove CV stains that was not absorbed by cells, and destaining of wells with 125 μL ethanol (95 %). A semi-quantitative evaluation of biofilm development was done by measuring $OD_{585\ nm}$ absorbance of 100 μL destaining solution transferred into a new plate, followed by calculation of the inhibitory effects of the extracts and standards using the parameters of 0 and 49 % (low activity) and 50 % or higher (high activity).

In testing for biofilm development inhibition, 50 μL MH broth and 50 μL of standardized *P. aeruginosa* culture were added to microtiter plates (Merck, South Africa) and allowed to form mature biofilm over 12–24 h incubation at 37 °C. Then 50 μL of extracts and standards at MIC to 1/8 MIC were added to wells in triplicates and the mixture incubated again for 24 h. The set up was stained with CV as in the cell attachment assay, followed by determination of inhibitory effects expressed as percentages and following parameters earlier described.

2.2.5. Pyocyanin inhibition assays

In the pyocyanin inhibition assay, 3 mL of standardized (0.08 at 600 nm) broth culture of *P. aeruginosa* was added into sterile 15 mL centrifuge tubes. Then, different concentrations of standards and plant extracts (MIC to 1/8 MIC) were added to the standardized culture prepared in King's A broth and incubated at 37 °C for 18–24 h. Thereafter, 1.5 mL of this culture was transferred into sterile Eppendorf tubes and centrifuged for 10 min at 3000 × *g*. Then about a mL of supernatant was pipetted into fresh sterile tubes that had been pre-cooled in ice, followed by addition of chloroform (100 μL) while on ice, and then hydrochloric acid (300 μL of 0.2 M). The reaction mixture was vigorously mixed, and the supernatant (chloroform layer into which pyocyanin is extracted) pipetted into a fresh microtiter plate, and absorbance measured at 520 nm. The pyocyanin concentration was determined by multiplying obtained ODs with the pyocyanin molar extinction coefficient of 17.072. The experiment was done in triplicates and compared to untreated control cells [22].

2.2.6. Confocal laser scanning microscopy (CLSM)

Biofilm quantification and imaging by Confocal Laser Scanning Microscopy (CLSM) was done to assess *P. aeruginosa* biofilm viability following exposure to extracts over a period of time. Biofilms were allowed to develop at 37 °C for 12 h on glass coverslip pieces of size 1 × 1 cm placed in a 24-well microtiter plate. After 12 h, formed biofilms were treated with the extracts and standards at their MICs in duplicate, with incubation for 24 h. Attached biofilms were gently rinsed using deionized water, stained with backlight viability kit (containing propidium iodide and Syto 9 fluorescence), incubated in a dark area for 15 min, followed by one-time plate wash and viewing of fluorescence using a Zeiss LSM 510 (Germany) confocal microscope. Laser emission collection was done with a 500–530 bandpass filter and excitation achieved at 488 nm [32].

2.3. Untargeted chemometric profiling of the extracts

The metabolomic profiles of the extracts derived from six *H. annuus* seed cultivars were analysed by the Ultra-High Performance Liquid Chromatography (UHPLC-MS) [33]. After 1 h ultrasonication (Bransonic, USA), resulting supernatants were transferred into respectively labelled amber coloured glass vials for each extract. Samples were then analysed using the Waters Synapt G2 Quadrupole Time-of-Flight (QTOF) Mass Spectrometer (MS) connected to a Waters Acquity UHPLC-MS (Waters, Milford, MA, USA) for high-resolution metabolomic analysis. Data was acquired with a *m/z* scan range of 150 to 1500 in resolution mode, as well as in msE mode acquisition with the Synapt G2. Compounds detection and confirmation was cone with MSDIAL, MSFINDER (RIKEN Centre for Sustainable Resource Science: Metabolome Informatics Research Team, Kanagawa, Japan). The metabolomic profiling method used covered for identical precursor ions (isomers) detection

and differentiation using chromatographic separation and matching fragmentation patterns. In metabolomic multivariate analysis, the generated data was first sample median normalized, log transformed, and Pareto-scaled. The heat map, partial least squares discriminant analysis (PLS-DA) and principal component analysis (PCA) plots (to analyse consistency of key metabolites) were generated with MetaboAnalyst 6.0 (https://www.metaboanalyst.ca, accessed on 15 October 2023) [34].

2.4. In silico determinations

2.4.1. Molecular docking and fingerprinting

The 3D structure of *P. aeruginosa* LasR protein (PDB ID: 2UV0, sequence length of 175) was downloaded from the Protein Data Bank (https://www.rcsb.org/, accessed on 15 August 2023) in protein data bank (pdb) file format. The ligands [*H. annuus* metabolites identified from UHPLC-MS, and standards (azithromycin, cinnamaldehyde)] were downloaded from PubChem (https://pubchem.ncbi.nlm.nih.gov/, accessed on 15 August 2023) in simple data file (sdf) format. The protein and respective ligands were optimized for docking analysis using UCSF Chimera version 1.15 [35]. Molecular docking was conducted using PyRx v 0.8 [36] embedded with AutoDock vina to find the best binding poses characterized by lowest docking scores [37]. Molecular fingerprinting of the top 10 metabolites with the lowest docking scores was done using Galaxy Europe (https://usegalaxy.eu./#, accessed on 13 October 2023) [38] to assess the levels of structural variability across the identified lead compounds, which assisted with streamlining to the top 5 based on conformation with the Lipinski's rule of 5 (Ro5) and synthetic scores <5 [39].

2.4.2. Pharmacokinetic features analyses

The top 5 ligands with the best poses or docking scores from molecular docking with *P. aeruginosa* LasR protein and identified from molecular fingerprinting were subjected to the SwissADME server tool (https://www.swissadme.ch/, accessed 13 October 2023) to estimate their pharmacokinetic and physicochemical [absorption, distribution, metabolism, excretion (ADME)] properties [39].

2.4.3. Molecular dynamics (MD) simulation and post-dynamic analyses

The top 5 metabolites complexed with the LasR protein were subjected to MD simulation using the graphics processing unit (GPU) version of AMBER 18 to run FF18SB (variant) force field variant using the in-house module programme resident at the Centre for High Performance Computing, Cape Town, South Africa. The LasR protein sequence length of 175 was used, and simulation was done over 100 ns, and compounds' partial charges generated in an ANTECHAMBER using the general amber force field (GAFF) and restrained electrostatic potential (RESP) procedures. The AMBER 18 module permitted TIP3P water molecules, hydrogen (H) atoms, sodium (Na^+) and chlorine (Cl^-) counter ions addition to aid neutralization of system. Non-bond interactions threshold was set at 8 Å using ligand-assigned ANTECHAMBER charges. Each system hydrogen atom bonds were limited using the SHAKE technique and done in 2 fs steps, at isobaric–isothermal ensemble (NPT), randomized seeding, 1 ps collision frequency and 300 K [40,41]. In post-dynamic analyses, the CPPTRAJ program was used in trajectories processing to analyse for root-mean-square deviation (RMSD), root-mean-square fluctuation (RMSF), solvent-accessible surface area (SASA) and the radius of gyration (ROG). The calculation of complexes Gibb's free binding energies (ΔG_{bind}) over interval (30 ns, 60 ns, 100 ns) snapshots from a 100 ns simulation was done using the molecular mechanics and generalised Born surface area method (MM/GBSA) strategy [41]. All bond and amino acid residue interactions were thereafter analysed using version 21.1.0 of the BIOVIA Discovery Studio software [42] and post-dynamic parameter plots generated using Origin version 6 software [43]. Lastly, ligand–protein (amino acid residues) contact maps in form of histograms (amino acid residues plotted against interaction fraction) were generated for the top 3 metabolites and azithromycin to provide a summary on simulation interactions [44].

3. Results and discussion

3.1. H. annuus seed extracts' antibacterial activities

Antibacterial susceptibility assays showed that aqueous and hydro-alcoholic extracts derived from Pannar cultivars 7102, 7160, 7170 and 7180 cultivars had the highest inhibition zones ranging from 11 to 16 mm at 600 mg/mL, and 10–14 mm at 400 mg/mL (Supplementary Table S1). The standard FDA-approved quorum sensing inhibitor (QSI) antibiotic, azithromycin [27], showed a 15 mm inhibition zone, comparable to zone range of cultivar 7102, 7160, 7170 and 7180 cultivars' extracts (Supplementary Table S1). Extract MICs ranged from 25 to 100 mg/mL, with cultivars 7102 water and hydro-ethanol extracts having MIC values of 50 and 100 mg/mL, respectively. In comparison, the standards, azithromycin (0.25 mg/mL), and cinnamaldehyde (3.75 mg/mL) demonstrated notable MIC values, thus confirming their robust antibacterial capabilities (Supplementary Table S1). The extracts showed concentration-dependent, and low to significant antibacterial action with significant activity at ≥13 mm and low activity at 9–12 mm [45]. On the other hand, 7156 and 7158 cultivar extracts showed no inhibitory activity depicting no antimicrobial action. Similar observation was reported for *Melilotus elegans* hydroalcoholic extracts against *Staphylococcus aureus* [46]. Extracts biological activities have been linked to levels of key bioactive principles or phytochemical types expressed in plants fractions, which is closely associated with solvent type used [47]. Sunflower seed oils have been reported to show antibacterial action against *Bacillus subtilis*, *S. aureus*, and *Escherichia* coli microbes implicated in urinary tract infections (UTIs), with oil activity linked to their content of polyphenols and volatile compounds [48,49]. Also, despite the high MICs, a similar study by S'thebe and co-authors [19] recorded 91.80 mg/mL MIC for sunflower seed oils while investigating the oil's AQS property.

3.2. Qualitative and quantitative anti-quorum sensing determinations

3.2.1. Qualitative AQS

The extracts with best antibacterial activity were further tested for their quantitative and qualitative AQS potential against *C. violaceum* ATCC 12472, the QS inhibition bio-monitor strain known to produce the visually distinct purple violacein pigment [50]. This was done because no literature exists on the *H. annuus* Pannar seed cultivars studied and their ability to inhibit QS. Qualitative AQS analysis showed that extracts exhibited moderate AQS potential as opaque zones of concentration-dependent violacein inhibition (Supplementary Table S2) against *C. violaceum* ranged from 10 to 12 mm at sub-MIC concentrations. Extracts from the cultivar 7170 presented the best zones of inhibition (12–15 mm), while the 7180 aqueous extracts showed no inhibition. The reference standards, azithromycin and cinnamaldehyde showed inhibition zones of 15 mm (susceptible, inhibition of violacein >10 mm) and 5 mm (resistant, inhibition of violacein ≤10 mm) (Supplementary Table S2), respectively. An earlier study on sunflower seed oil AQS activity also recorded low qualitative inhibition of violaceum as depicted by small inhibition zones. This could be attributed to the resistance of *C. violaceum* to the extract which may result in reduced therapeutic effect at higher doses [19]. The inability of PAN 7180 aqueous extract to show AQS effect could be due to the inappropriateness of solvent used [51], the sunflower's ontogenetic cycle and growth and development events that reduce the seed cultivar's key bioactive metabolite levels [17]. Treatment of *C. violaceum* with extracts may have influenced violacein pigment production, suggesting potential inhibition of the microbe's QS system, as observed from opaque zones around diffusion wells and reduced expression levels of violacein. However, given the preliminary outcomes, qualitative violacein inhibition does not always

suffice as the best AQS validation technique. As such, quantitative AQS test was further explored in results validation.

3.2.2. Quantitative AQS

The *H. annuus* extracts displayed varied AQS action against *C. violaceum,* as evidenced by their substantial reduction in violacein production (≥50 % equals good or high activity) following treatment at MIC and sub-MICs, with best inhibitory effect observed in the order of cultivars 7102 > 7180 > 7170 > 7160 (Supplementary Fig. S2). All extracts displayed violaceum inhibition at a decreasing exponential rate but PAN 7102 hydroalcoholic extract showed relatively reduced effect across all concentrations. Consistent with the qualitative AQS results, the PAN 7102 cultivar water extract also showed the highest inhibitory potential (74.26 %), followed by its hydroethanolic extract (73.16 %) and 7180 hydroethanolic extract (70.95 %). Interestingly, these extracts showed a much more significant inhibitory potential than azithromycin (66.71 %) and cinnamaldehyde (63.23 %). These findings align with a previous study reporting up to 50 % violaceum inhibition for Chinese herbal extracts which was indicative of extracts being able to inhibit acyl-homoserine lactone (AHL) binding to the CviR transcriptional regulator in *C. violaceum* [13,52]. The absence of inhibition by the hydro-ethanolic extract of 7170 at 1/8 sub-MIC may be due to limited availability of bioactive metabolites and excess dilution resulting in the bacterium's reduced sensitivity at lower concentrations and minimal or no inhibitory effects [53]. The reference standards also showed good violacein inhibition at all concentrations which reduced at sub-MIC levels. The structural semblance of the metabolites allows them to bind competitively to the *C. violaceum* CviR receptor protein in place of AHL, invariably disrupting QS signal transmission and further virulence factor expression [52]. These findings constitute a first-time validation of the quorum sensing inhibiting (QSI) capacity of the investigated Pannar *H. annuus* seed cultivars.

3.3. Impact of extracts on inhibition of swimming and swarming motility

The anti-swarming and swimming motility effects observed after treating *P. aeruginosa* cells with the extracts are noteworthy, showing significant difference within treatment groups, and increased inhibition within reducing MICs (Fig. 1a and b). The results showed that all plant extracts, especially PAN 7102 cultivar hydroalcoholic extract performed consistently well, reducing swimming and swarming in *P. aeruginosa* in a way that surpassed the performance of reference standards. A noticeable decrease in the diameter zone was observed for all extracts at reducing concentrations, indicating significant inhibition of motility compared to untreated cells. These outcomes emphasize the significant potential interference of extracts' metabolites in the inhibition of QS-associated virulence factors like microbial mobility and toxins expression [54]. The findings are also in alignment with earlier studies reporting inhibited swarming in *C. violaceum* following treatment with *Passiflora edulis* ethyl acetate fractions [53], and reduced swimming and swarming in *P. aeruginosa* after cells treatment with *H. annuus* oils [19]. Hence, since motility in P. aeruginosa is crucial to its pathogenicity and

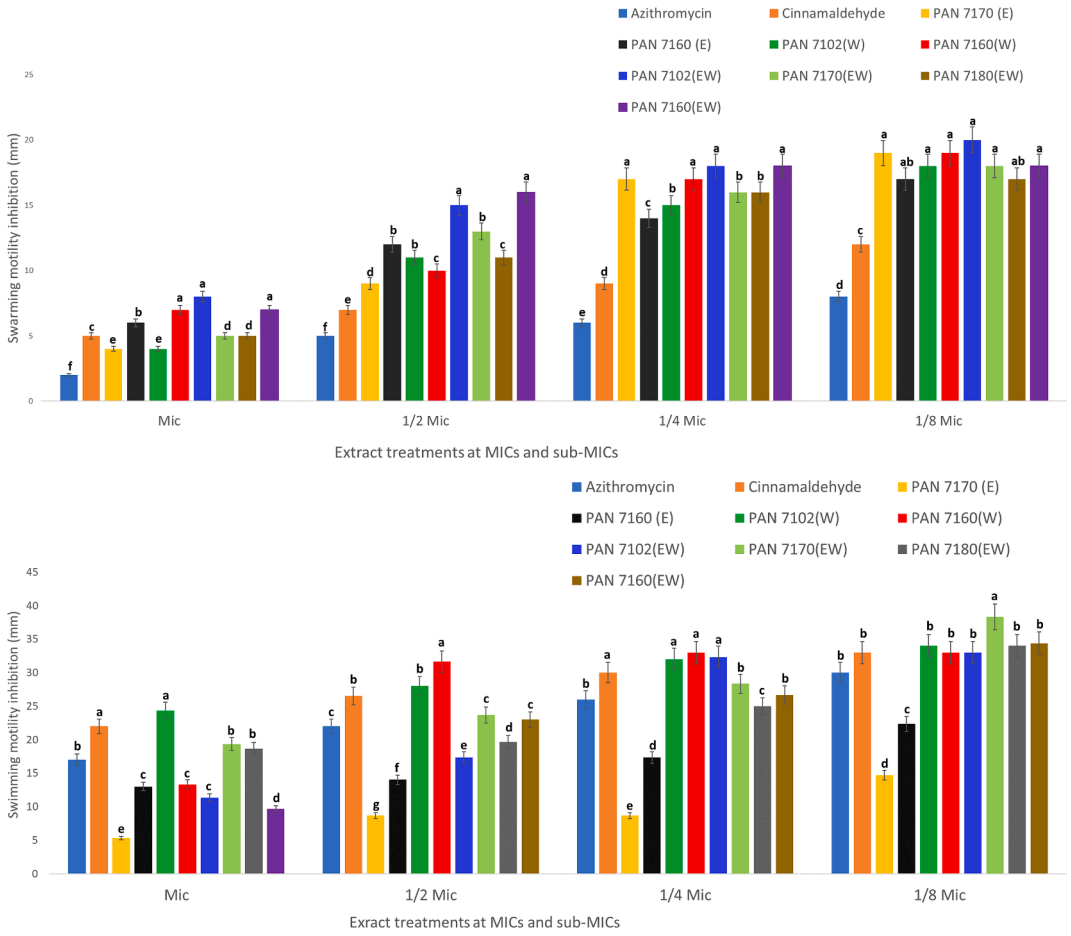

Fig. 1. (a) Inhibitory effect of active *H. annuus* extracts on *P. aeruginosa* swarming. PAN = Pannar cultivar; E = ethanol, W = water, EW = hydroethanol, Mic = minimum inhibitory concentration. [a-f]Values are mean ± SD of replicates, and within each group different letters/superscripts indicate significant difference ($p < 0.05$). (b) Inhibitory activity of active *H. annuus* extracts on *P. aeruginosa* swimming motility. PAN = Pannar cultivar; E = ethanol, W = water, EW = hydroethanol, Mic = minimum inhibitory concentration. [a-g]Values are mean ± SD of replicates, and within each group different letters/superscripts indicate significant difference ($p < 0.05$).

virulence, and ability to form biofilms, restricting its mobility could contribute to attenuating the microorganism's virulence. This holds significance for added exploration of *H. annuus* wild and hybrid cultivars in industrial medical settings.

3.4. Inhibition of cell attachment, biofilm and pyocyanin production

3.4.1. Cell attachment and biofilm inhibition potential of H. annuus fractions

The extracts competed favourably with the reference standards in inhibiting *P. aeruginosa* cell attachment and biofilm formation in a concentration dependent manner (Fig. 2a and b). At MIC, seed extracts had cell attachment inhibitions ranging from 50 to 88 %, while azithromycin and cinnamaldehyde elicited 67 % and 66 % inhibition, respectively. The 7102 water and hydroethanolic extracts displayed the best *P. aeruginosa* attachment inhibition at 88 % and 83 %, respectively, followed by the 7160 aqueous extract (80 %). Extracts from Pannar cultivars 7170 and 7180 also displayed high attachment inhibitory activities >50 %. Notably, all extracts at MIC to ¼MIC values showed greater than 50 % cell attachment inhibition suggesting that their inherent metabolites may have anti-QS properties (Fig. 2a). The ability of the seed extracts to interfere with the cell attachment, a precursor stage in *P. aeruginosa* biofilm development may be attributed to interference with electrostatic interaction and Lifshitz–Van der Waals forces that favour bacterial cells adherence to surfaces during the initial stages of infection progression [55]. The Pannar seed cultivars' extracts may hold promise for the reduction of colonization capacity on surfaces and body epithelial cells, thereby preventing infections. A similar observation was made in a previous study done by Famuyide et al. [31] where crude ethanolic and acetonic *Psidium guajava* fractions prevented *Streptococcus mutans* cell attachment. Biofilm inhibition was concentration dependent for all tested *H. annuus* extracts, with relative increase in inhibition at lower concentrations. The 7160 water (67.52 %) and ethanolic (68 %) extracts displayed the highest inhibitory potentials which were relatively comparable to azithromycin (67.85 %) and cinnamaldehyde (66.55 %) the reference standards, all showing acceptable biofilm inhibiting activities (Fig. 2b). Walmiki et al. [56] also reported on the biofilm inhibitory capacities of *Piper nigrum*, *Syzygium aromaticum* and *Cuminum cyminum* oils against selected pathogenic bacteria. Also, azithromycin may have performed better that the extracts in inhibiting biofilm formation due to it being a standard, modified or refined QSI antimicrobial agent [27]. Hence, Pannar seed cultivars' extracts may contain one or more metabolites with anti-QS and anti-biofilm inhibition properties.

3.4.2. Assessing pyocyanin expression inhibition

In the case of pyocyanin production, results depicted in Supplementary Fig. S3 indicated a consistent reduction in pyocyanin production in a trend that was dependent on concentration upon introduction of standards and seed extracts into the bacterial cell culture. Extracts pyocyanin production inhibition ranged from 58 to 78 %, competing favourable with reference standards inhibition. The PAN 7102 cultivar

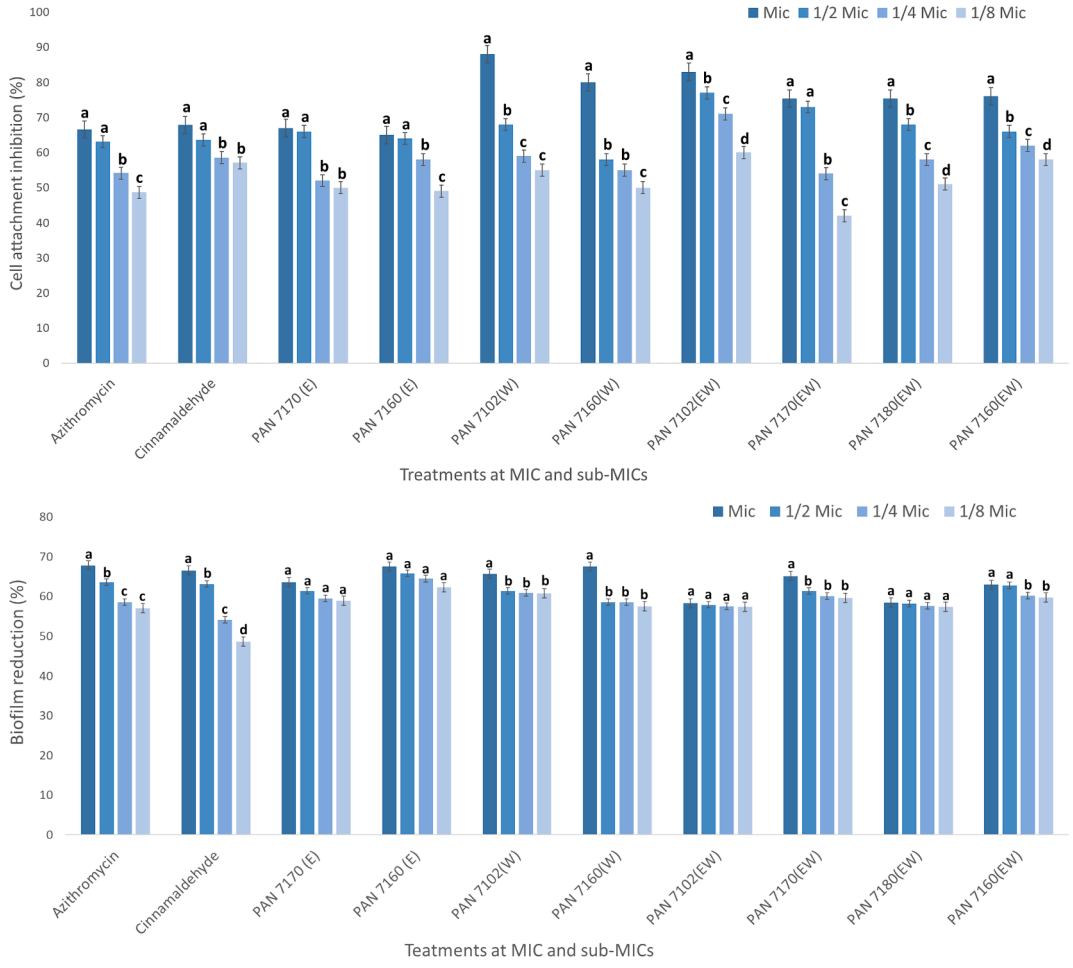

Fig. 2. (a) Inhibitory activity of *H. annuus* extracts on *P. aeruginosa* cell attachment. PAN = Pannar; E = ethanol, W = water, EW = hydroethanol, Mic = minimum inhibitory concentration. [a-d]Values are mean ± SD of replicates, and within each group different letters/superscripts indicate significant difference ($p < 0.05$). (b) Inhibitory activity of *H. annuus* extracts against biofilm formation in *P. aeruginosa*. PAN = Pannar; E = ethanol, W = water, EW = hydroethanol, Mic = minimum inhibitory concentration. [a-d]Values are mean ± SD of replicates, and within each group different letters/superscripts indicate significant difference ($p < 0.05$).

water fraction showed a 74 % inhibitory potential followed by the 7160 water (67.52 %) and hydroethanolic (62.98 %) extracts, 7170 hydroethanolic (65.15 %) and 7180 (62 %) extracts. Extracts' inhibitory potential at MIC values were higher than for the reference standards suggesting that *H. annuus* Pannar cultivar seed extracts contain key molecules with anti-QS activity and could function in modulating the *rhl* system that is a subset QS pathway regulated by the *P. aeruginosa* LasR system. These observations align with those of Chong et al. [13] where demonstrable reduction in pyocyanin expression was reported upon treatment of *P. aeruginosa* cell cultures with herbal extracts derived from four Chinese plant species. As a secondary phenazine metabolite and virulence factor, pyocyanin helps to induce free radicals' production in *P. aeruginosa* for onward interference with ion transport in host respiratory epithelial cells [57].

3.5. Validating biofilm inhibition by confocal laser scanning microscopy (CLSM)

To assess biofilm matrices further quantitatively and confirm the extent of biofilm inhibition by the investigated extracts, CLSM imaging was done. The ethanolic, water and hydroethanolic extracts of 7102 and 7160 cultivars showed the best anti-biofilm activities (Fig. 3d–h). The micrographs showed notable reduction in biofilm thickness for the extracts'-treated cells, compared to untreated cells which showed clumped up biofilms/cell aggregates (Fig. 3c). Also, despite the significant inhibition of biofilm biomass and thickness observed for azithromycin and cinnamaldehyde-treated cells (Fig. 3a and b), the extracts performed favourably well in inhibiting biofilm production (Fig. 3d–h). This observation may be linked to the standards being present in their bioactive, pure, concentrated and/or structurally modified forms, compared to the extracts that did not have the exact bioactive component(s) causing biofilm inhibition identified and present at optimal concentration. These findings confirm the results from cell attachment and biofilm inhibition assays which point to the AQS activity of the *H. annuus* extracts.

3.6. Metabolomic bioprospection of H. annus seed extracts

3.6.1. Metabolomic profiling and analysis

The chemometric PCA score plot of the metabolomic data unveiled a substantial variance of 52.5 % across the six Pannar cultivars, thus emphasizing their distinct metabolite signatures (Fig. 4a). The PLS-DA plot (Fig. 4b) further demonstrated a 46.9 % variance, and complemented PCA in highlighting extract and cultivar-specific metabolomic differences. Pannar cultivars 7102, 7160 and 7156 aqueous and ethanol extracts were responsible for driving most of the observed feature (metabolite) variations in PC1, and the second highest amount of variance (PC2) among samples. Again, the PCA plot showed unique features for the 7102 A, 7102 E, 7160 MF, 7156 E, and 7158 A samples. The component 2 axis in the PLS-DA plot showed that cultivar extracts belonging to 7102 A, 7160 EA, and 7156 A had features specific to them. These sample accounted for the variation and clustering observed across all sample groups and metabolites. Intersecting (similar) features were observed across all cultivar MF extracts, as well as all 7170 and 7180 extracts. This indicated similar metabolome composition across the implicated cultivars. Samples were relatively closely clustered, yet separate indicating a high degree of metabolomic variation across cultivars. Although, the PLS-DA is useful in showing intra-cultivar differences, it depicted a lower degree of metabolites variance compared to inter-cultivar extracts' similarities. The observed higher variance score from PCA relative to PLS-DA could be attributed to smaller PCA (lower cross cultivar similarity) and larger PLS-DA clustering. The larger the cluster and spatial arrangement of key features, the greater the intra-cluster variation and vice versa [58]. Likewise, the PLS-DA supervised model is reported to usually overfit data points much more than PCA [59]. In addition, the associated heatmap shows the relative abundance of *H. annuus* metabolites across the six Pannar seed cultivars. The red boxes signify higher mean abundance/concentrations in samples, while the blue boxes indicate comparatively lower concentrations (Fig. 5). Hierarchical clustering included 24 analytical replications and the top 25 metabolite features grouped in a row. Higher metabolite intensities of aromatic phenol carboxylic acids (caffeic, and chlorogenic acids), dihydroisocoumarin phytoalexin (methoxymellein), quinic acid derivative (caffeoyl methylquinic acid), glycosyloxyisoflavone (formononetin

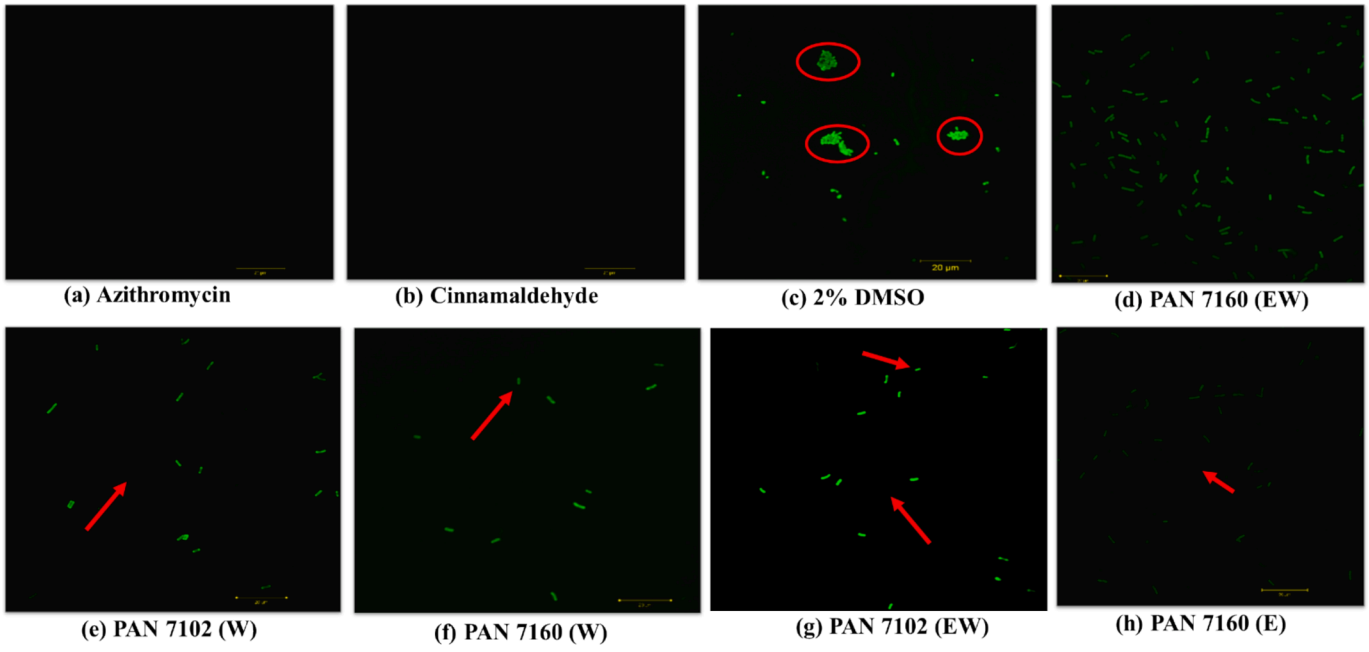

Fig. 3. (a–h) Confocal microscopy images of the antibiofilm efficacy of the most active *H annuus* extracts. Arrows = areas of clearing and isolated single cells (non-aggregated biofilms). Circle = areas of biofilm clumps. Pannar cultivars; PAN 7102 CLP, PAN 7160 CLP; E = Ethanolic extract, EW = Hydroethanol extract, W = Water extract.

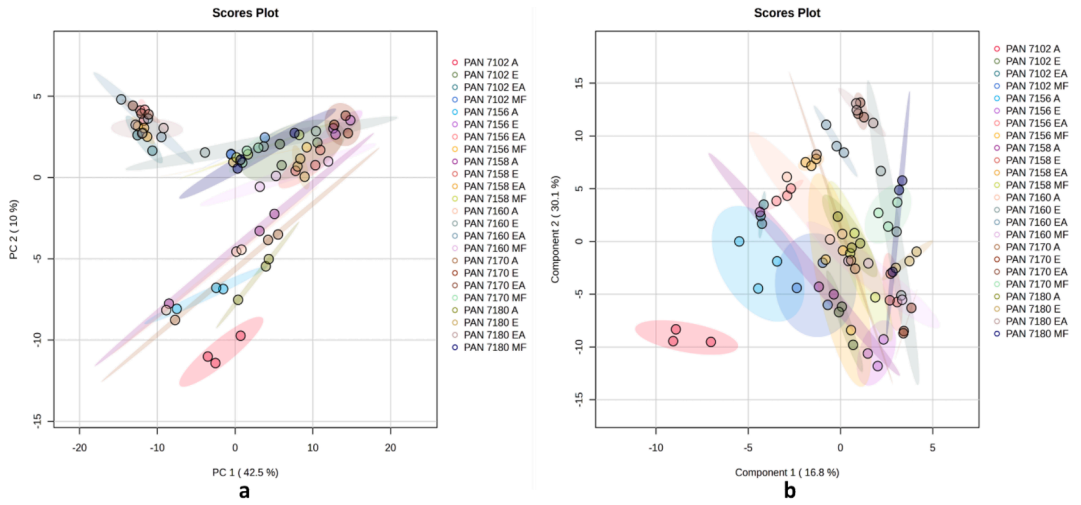

Fig. 4. Metabolites variation across six Pannar *H. annuus* seed cultivars using (a) PCA and (b) PLS-DA plots. Pannar cultivars; PAN 7102 CLP, PAN 7156 CLP, PAN 7158 HO, PAN 7160 CLP, PAN 7170, PAN 7180 CLP; Extraction solvents = water (A), ethanol (E), hydro-ethanol (EA) and acidified methanol extract (MF).

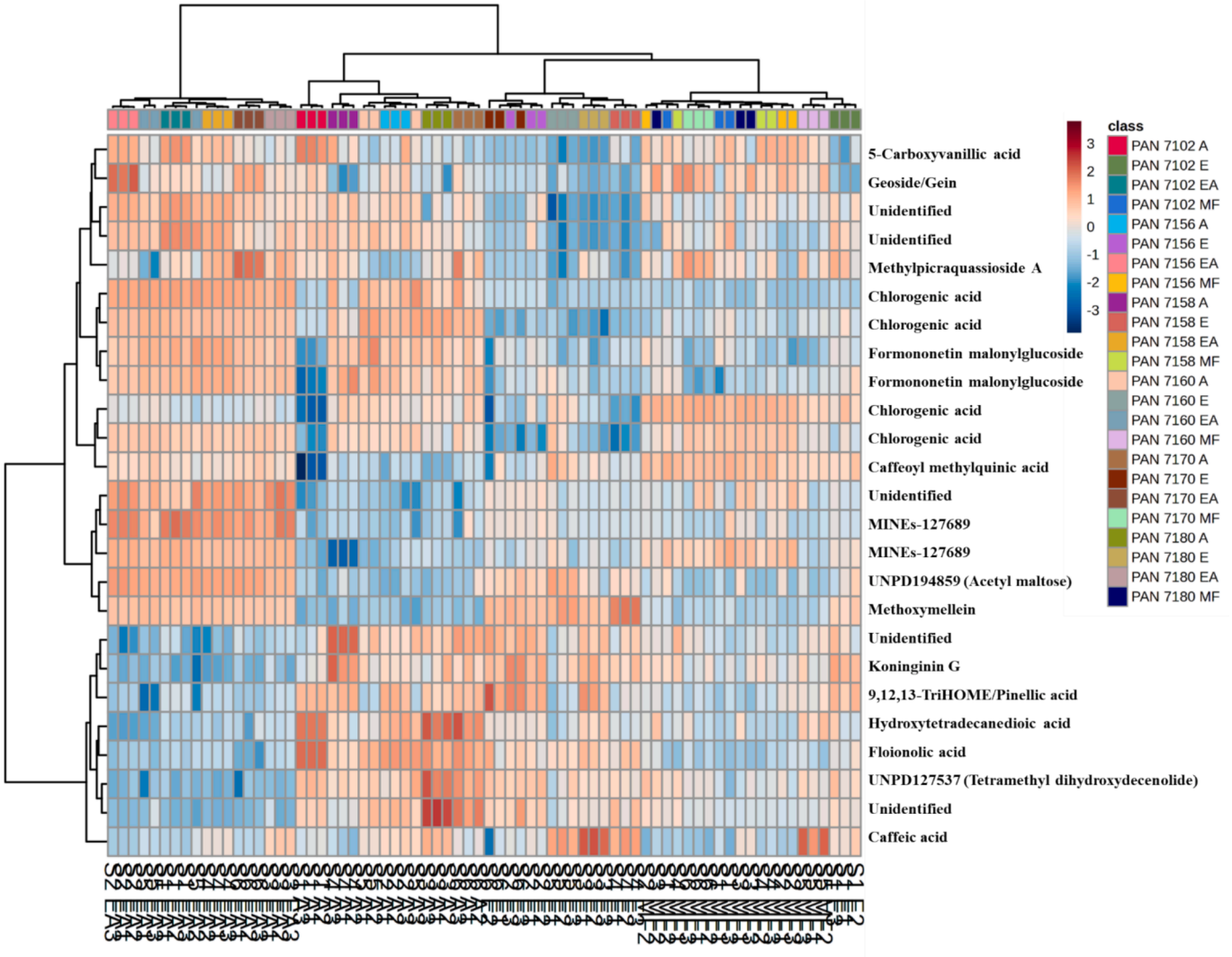

Fig. 5. Relative abundance heat map of 25 key features (compounds) across all *H. annuus* extracts. Pannar cultivars = PAN 7102 CLP, PAN 7156 CLP, PAN 7158 HO, PAN 7160 CLP, PAN 7170, PAN 7180 CLP; Extraction solvents = water (A), ethanol (E), hydro-ethanol (EA) and acidified methanol extract (MF); S1 = PAN 7102, S2 = PAN 7156, S3 = PAN 7180, S4 = PAN 7158, S5 = PAN 7160, S6 = PAN 7170.

malonylglucoside), and fatty acid (floionolic acid) were observed across all extracts, especially in ethanol, hydroethanolic and aqueous extracts of PAN 7102, 7160, 7158, 7156 cultivars, while some features were unidentified. These findings are in alignment with those made from unsupervised PCA and supervised PLS-DA models for same cultivars/extracts groups. The presence of phenolic and flavonoid compound derivatives in wildtype sunflower sprouts and seeds [15] and Armavireo variety sunflower seed meals [60], as well as fatty acids in Agsun seed oils [19] had earlier been reported. For the first time, this study reports the presence of methoxymellein, hydroxytetradecanedioic acid, koninginin G, geoside (a eugenol vicianoside), 9,12,13-TriHOME or pinellic acid, and a phenolic glycoside (methylpicraquassioside A) in *H. annuus* Pannar seed cultivars. The relatively uniform colour coding suggests good data reliability and reproducibility. The analysis of selected clustered feature hierarchies could be used in differentiating seed cultivar metabolomic fingerprints [58]. Metabolomic variation across plant variants of the same or different species have been linked to their ability to adapt and respond to prevailing environmental or locational elicitors that determine quantitative and qualitative metabolomic shifts and profiles. Such metabolomic elicitations are central to plant natural products bioprospection drives focused on new drugs discovery [61]. Overall, our observations regarding the metabolites of the investigated cultivars point to the efficacy of aqueous, alcohol, and hydroalcoholic solvents in enhancing the expression of similar and distinct metabolites during extraction, an attribute that is linked to their polarity index [20]. As such, the presence of distinct variables identified across Pannar cultivar and extract replicates emphasize the relevance of using varied solvents in sample extraction for untargeted metabolomics. This would enhance coverage in profiling outcomes, either for known or new plant species, or cultivar hybrids. Our findings show high feature variability across and within Pannar seed cultivars and provide first-hand valuable insights into metabolite diversity, similarity and distribution across hybrid Pannar cultivars. This thus laid a foundational metabolome baseline which could be built on in future research efforts to expand exploration of the seeds beyond food and oil uses.

3.6.2. *In silico metabolomic bioprospection*

3.6.2.1. Molecular docking, metabolites ranking, and interactions analysis. The metabolites identified through UHPLC-MS were used to build

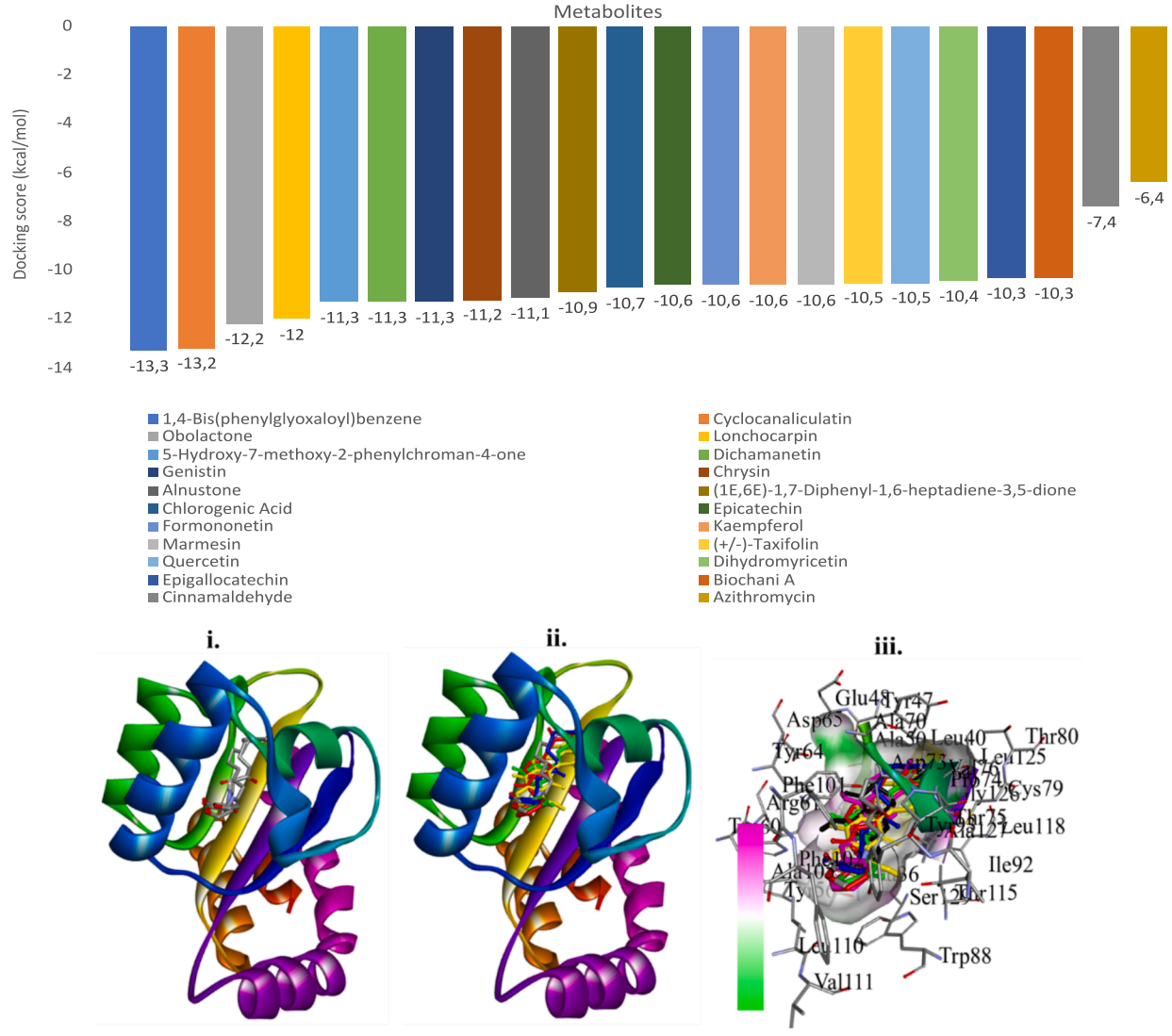

Fig. 6. (a) Docking scores of the top 20 metabolites from *H. annuus* and standards against *P. aeruginosa* LasR. (b) 3D docking validations (i) re-docking of co-crystal native ligand, (ii) superimposition of lead *H. annuus* metabolites (ligands), and (iii) key interacting residues (Tyr56, Trp60, Asp73, Thr75, Trp88, Tyr93, Ser129) from lead ligands superimposition at the LasR active site. Native ligand (3-oxo-C12-HSL, Blue), 1,4-bis(phenylglyoxaloyl) benzene (Red), cyclocanaliculatin (Yellow), Obolactone (Green), Lonchocarpin (Pink), 5-Hydroxy-7-methoxy-2-phenylchroman-4-one (Black). (For interpretation of the references to colour in this figure legend, the reader is referred to the web version of this article.)

a library of compounds and subjected to molecular docking to identify putative leads implicated in the observed effects of the extracts towards *P. aeruginosa* LasR protein. The top 20 metabolites had docking scores ranging from −13.3 to −10.3 kcal/mol, with the lowest docking scores observed for 1,4-bis(phenylglyoxaloyl) benzene (−13.3 kcal/mol). All 20 compounds had lower docking scores relative to the higher docking score observed for azithromycin (−6.2 kcal/mol) and cinnamaldehyde (−7.4 kcal/mol) (Fig. 6a). The docking protocol was validated by re-docking of the native ligand [N-3-oxododecanoyl homoserine lactone (3-oxo-C12-HSL)] (Fig. 6bi) and superimposition of lead metabolites at the LasR active site to derive an RMSD of less than 0.5 (Fig. 6bi–iii). All ligands were well fitted and docked in the LasR active site and interacted with key conserved (Tyr56, Trp60, Asp73, Ser129) and other hydrophobic (Leu36, Gly38, Leu40, Tyr47, Arg61, Thr75, Trp88, Tyr93, Phe101, Gly126) amino acid residues, forming strong bonds (Fig. 6biii), much like the native AHL ligand (3-oxo-C12-HSL). This suggests that the metabolites may act as native AHL mimics for competitive inhibition of LasR. In contrast to our findings, Dalal et al. [62] reported lower docking scores for two lead hygrophorones [A14 (−8.7 kcal/mol), A12 (−9.1 kcal/mol)] with LasR inhibiting potential. Nevertheless, the leads also formed stable Pi, alkyl and hydrogen bond interactions with Leu36, Tyr47, Tyr56, Trp60, Trp88 and Phe101. This observation was is in line with docking interactions for the leads reported for the first time in this present study. In contrast, diadzein and fridamycin A, lead compounds derived from termite-associated fungi did not interact with key LasR residues but formed hydrophobic bonds with Tyr87, Leu104 and Ser123 [63]. Such varied interactions for same protein targets point to the empirical nature of binding affinity measurements using docking scores that depend on enthalpy- or entropy-based binding and impact intermolecular electrostatic interactions [64].

The 2D and 3D ligand–protein interactions for the 5 lead *H. annuus* metabolites were also depicted in Supplementary Fig. S1. Docking scores were used in selecting the best-posed metabolites (ligands) within the active site pocket of LasR. Thereafter, molecular fingerprinting analysis was done using the top 10 compounds with highest docking scores to further aid streamlining to the top 5 metabolites (Supplementary Fig. S4) using leads 3D complementary molecular features. Structure-based fingerprinting provided added credence to its use, efficiency, and specificity in lead ligands substructure analysis, and findings are consistent with the reports of Cai et al. [65], and Koes and Camacho [66]. However, based on the observed potential binding affinities, the pharmacokinetic attributes of the identified 5 lead metabolites [1,4-bis (phenylglyoxaloyl)benzene, cyclocanaliculatin, obolactone, lonchocarpin, and 5-Hydroxy-7-methoxy-2-phenylchroman-4-one] were further investigated.

The analysis of pharmacokinetic attributes using the ADME tool serves to reduce the probability of obtaining false-positive outcomes linked to *in vivo* and *in vitro* validation. Following pharmacokinetic features prediction, the top 5 *H. annuus* metabolites were shown to conform to the Lipinski Ro5 (Table 1). The attributes included their ability to penetrate the cell membrane, high bioavailability, lipophilicity, and low to high gut absorption properties, compared to the azithromycin standard which violated two drug-likeness criteria (hydrogen bond acceptors >10, molar weight >500). The 5 lead metabolites showed moderate to high solubility, with obalactone showing the highest bioavailability or water solubility score. A lipophilicity (log P) scores of ≤5 indicates that a compound is readily miscible in a lipid (oil) rather than in an aqueous phase. This suggests a strong ability to be absorbed and permeate the cell membrane [67]. A high gut absorption attribute indicates a metabolite's intestinal absorption and permeability features [68]. The Ro5 states that compounds with ≤2 violations will not be bioavailable when taken orally. Thus, the identified lead *H. annuus* compounds could be developed into orally bioavailable drug formulations for effective pharmacological modulation of LasR [69,70].

3.6.3. Energy component, molecular dynamics (MD) and post-dynamics analysis

In thermodynamic energy component analysis, the binding free energy (ΔG_{bind}) reflects the energy difference between the unbound receptor and bound complex (using 100 ns MM/GBSA computations), and indicates a molecule's affinity for the target and bond strength [71]. The ΔG_{bind} value is an enhanced scoring function that supersedes the docking score in showing the affinity of a ligand for its target. A lower or more negative ΔG_{bind} values indicates better complex stability and affinity. Obolactone (−48.26 ± 3.56 kcal/mol), followed by 1,4-bis(phenylglyoxaloyl)benzene (−45.06 ± 2.95 kcal/mol) and cyclocanalucilatin (−43.41 ± 4.15 kcal/mol) had the lowest ΔG_{bind} compared to the standards azithromycin (−32.09 ± 1.55 kcal/mol) and cinnamaldehyde (−16.64 ± 1.82 kcal/mol) (Table 2). Similar to our findings for obolactone, 1,4-bis(phenylglyoxaloyl)benzene and cyclocanaliculatin, Sadiq et al. [72] also reported MMGBSA measured ΔG_{bind} of −44.23 kcal/mol for sulfadiazine and −46.27 kcal/mol for articaine, both FDA-approved drug leads repurposed as LasR antagonists. Hence, findings from our ΔG_{bind} outcomes for *H. annuus* leads showed comparable and enhanced binding affinity for LasR. These findings suggest their better potential as novel modulators of *P. aeruginosa* LasR.

Furthermore, the thermodynamic stability of the 5 lead *H. annus* metabolites complexed with the LasR were assessed by evaluating their trajectories (Fig. 7a–d, Supplementary Table S5) over a 100 ns MD simulation period. The RMSD is used to measure complex structure divergence compared to the apo-protein (protein in its free form and unbound to any ligand). Lower deviation values indicate increased complex stability [73]. In this study, following convergence of complexes at 5 ns, each system shows minimal sway and remained relatively stable and equilibrated up to 60 ns. From 60 to 100 ns greater flux and increase in RMSD was observed, with obolactone-LasR (1.38 ± 0.19 Å)

Table 1
Pharmacokinetic properties of the top 5 performing *H. annuus* compounds.

Ligand	Mol. Weight (≤500 g/mol)	HBD (≤5)	HBA (≤10)	Lipophilicity (LogP ≤5)	Bioavailability (water solubility)	GIT absorption	Drug-likeness (Lipinski Violations)
1,4-bis(phenylglyoxaloyl) benzene	342.34	0	4	1.91	0.55 (moderately soluble)	High	Yes (0 violation)
Cyclocanaliculatin	360.32	1	6	1.93	0.55 (moderately soluble)	High	Yes (0 violation)
Obolactone	310.34	0	4	2.95	0.85 (soluble)	High	Yes (0 violation)
Lonchocarpin	306.36	1	3	3.49	0.55 (moderately soluble)	High	Yes (0 violation)
5-Hydroxy-7-methoxy-2-phenylchroman-4-one	270.28	1	4	2.75	0.55 (soluble)	High	Yes (0 violation)
*Cinnamaldehyde	132.16	0	1	1.97	0.55 (soluble)	High	Yes (0 violation)
*Azithromycin	748.99	5	14	2.02	0.17 (poorly soluble)	Low	No (2 violations: MW > 500, NorO > 10)

HBD = hydrogen bond donor, HBA = hydrogen bond acceptor, GIT = gastrointestinal tract; MW/Mol. Weight = molecular weight, *Cinnamaldehyde and azithromycin = reference (positive controls) molecules.

Table 2
Energy components (kcal/mol) of lead compounds after 100 ns MD simulation.

Target	Ligands	ΔE_{vdW}	ΔE_{elec}	ΔG_{gas}	ΔG_{solv}	ΔG_{bind}
LasR (2UV0)	*Azithromycin	−24.92 ± 1.10	−251.04 ± 5.08	−289.23 ± 6.08	257.14 ± 5.76	−32.09 ± 1.55
	*Cinnamaldehyde	−22.77 ± 1.83	−14.22 ± 2.94	−36.99 ± 2.78	20.35 ± 2.14	−16.64 ± 1.82
	N-butyryl homoserine lactone	−30.23 ± 3.26	−28.03 ± 9.80	−58.27 ± 7.75	28.56 ± 5.58	−29.71 ± 3.01
	Obolactone	−52.10 ± 2.89	−26.98 ± 3.88	−79.08 ± 4.71	30.82 ± 2.47	**−48.26 ± 3.56**
	Lonchocarpin	−43.68 ± 3.23	−14.72 ± 4.97	−58.39 ± 6.05	24.62 ± 4.13	−33.78 ± 4.12
	Cyclocanaliculatin	−55.02 ± 3.05	−172.88 ± 1.17	−227.90 ± 1.58	184.49 ± 1.79	**−43.41 ± 4.15**
	5-Hydroxy-7-methoxy-2-phenylchroman-4-one	−41.59 ± 2.40	−18.82 ± 9.22	−60.42 ± 9.27	21.24 ± 3.97	−39.18 ± 5.80
	1,4-bis(phenylglyoxaloyl) benzene	−53.58 ± 2.94	−22.48 ± 4.98	−76.07 ± 4.41	31.00 ± 2.74	−45.06 ± 2.95

ΔE_{vdW} = van der Waals energy; ΔE_{elec} = electrostatic energy; ΔG_{gas} = gas phase free energy; ΔG_{solv} = solvation free energy; and ΔG_{bind} = total binding free energy.
*Cinnamaldehyde and azithromycin = reference (positive controls) molecules.

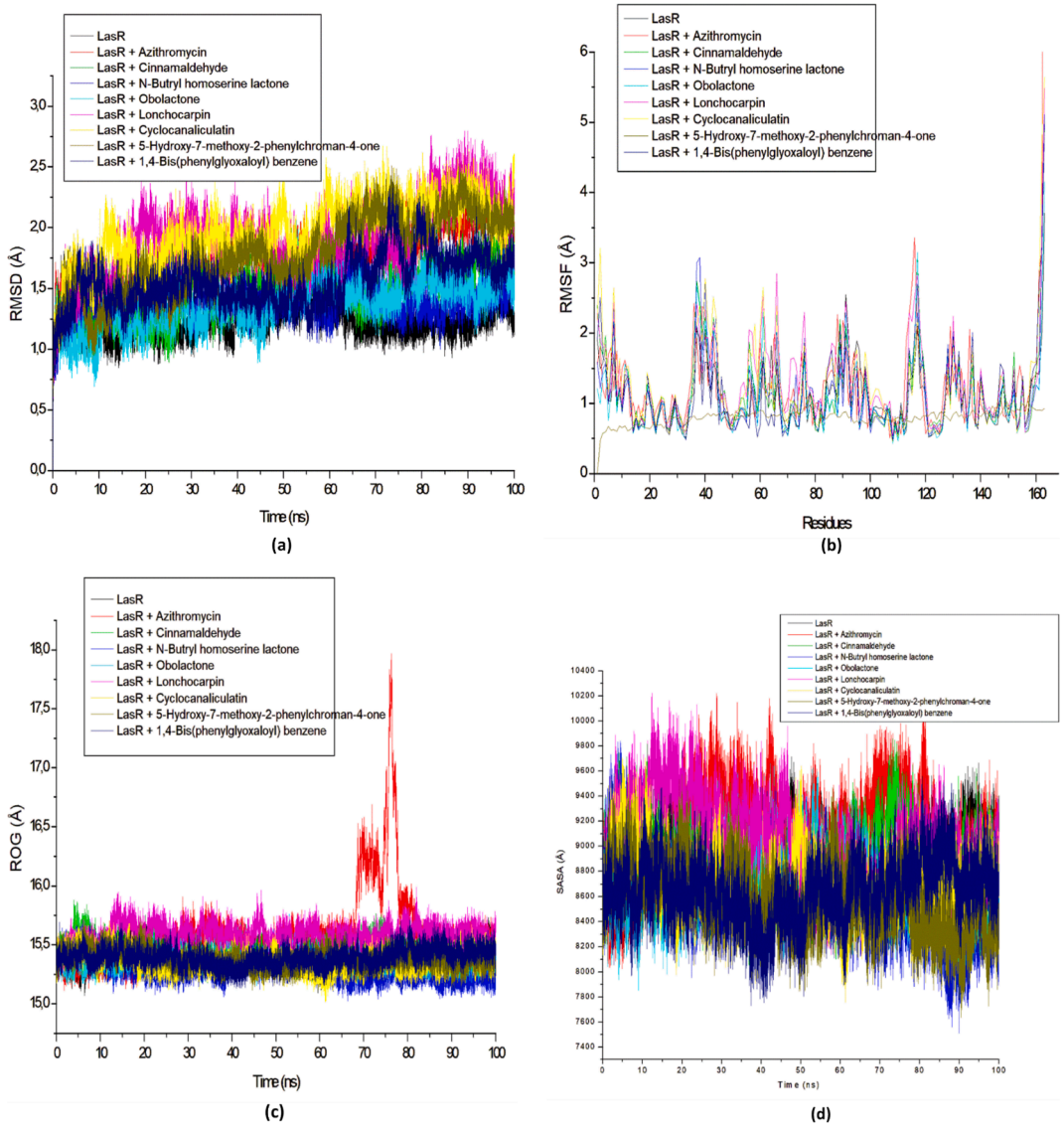

Fig. 7. Comparative plots of ligand–protein complexes represented as (a) RMSD (root-mean-square deviation), (b) RMSF (root-mean-square fluctuation), (c) RoG (radius of gyration), and (d) SASA (solvent-accessible surface area), over a 100 ns MD simulation period.

and 1,4-bis(phenylglyoxaloyl)benzene-LasR (1.56 ± 0.21 Å) systems showing minimal sway and better stability compared to other lead *H. annus* metabolite complex systems, and azithromycin-LasR system (1.75 ± 0.24 Å). In line with our observations, the work of Dalal et al. [62] also recorded no change in LasR protein structure following the binding of lead hygrophorones A14, A16 and D16 with RMSD values less than 0.5 nm during a 100 ns simulation time. Thus, of the top 5 metabolites identified in this study, obolactone and 1,4-bis(phenylglyoxaloyl)benzene had the lowest RMSD values, suggesting that both metabolites had a better advantage as modulators of LasR. The higher deviation value recorded for azithromycin depicted its reduced thermostability with the LasR target. Nonetheless, fluctuations for all metabolite-protein complexes remained within the 3 Å value showing the stability of their bound complexes, as well as the stable interaction of

ligands with amino acid residues at the target active site (Fig. 7a). Deviation values greater than 3 Å therefore indicated significant deviation from equilibration point and thermodynamic instability [74,75].

In quantifying the mean structural or residue areas that vary the least or most, the evaluation of RMSF values of complexed systems was done to shed light on the stability of intra- and intermolecular bonds formed with residues. Lower fluctuation of residues depicts stronger bonds formed [76]. Of the lead metabolites, obolactone-LasR, 5-hydroxy-7-methoxy-2-phenylchroman-4-one-LasR, and 1,4-bis(phenylglyoxaloyl) benzene-LasR systems had the lowest respective RMSF values of 1.09 ± 0.54 Å, 0.80 ± 0.11 Å, and 1.11 ± 0.58 Å. Higher residue fluctuations were observed in all systems across residues 35 and 45, 105 and 120, and 160 during MD simulation. This indicated a reduced ability of these residues to form stable bonds (Fig. 7b). The highest flexibility was observed across all standards and autoinducer molecules, while obolactone-LasR, 5-hydroxy-7-methoxy-2-phenylchroman-4-one-LasR, and 1,4-bis(phenylglyoxaloyl)benzene-LasR systems showed less atomic or residue flux. This suggested their better thermodynamic compatibility with the LasR target (Fig. 7b, Supplementary Table S5). The finding implies that the 3 lead compounds formed stable bonds (inter- and intermolecular bonds) with LasR active site residues which contributed to the thermodynamic flexibility and stability of their complexes [77]. Nonetheless, other complexed lead molecules (cyclocanaliculatin and lonchocarpin) also had mean RMSF values less than 3 Å and were relatively stable. In agreement with our findings, a LasR + curcumin system was reported to show a reduced mean local flux of ≤3 Å. This depicted thermodynamic stability irrespective of ligand binding [78]. Using the Gromacs 2022.2 version, another study recorded a low mean flux across all amino acid residues (between 0.14 and 0.4 nm) for the LasR + chrysin system which showed stability of the lead ligand structure within the LasR binding site [79]. The evaluation of fluctuations in protein residue configurations has integral functions in determining affinity and orientation changes that occur in macromolecular complexes [80]. Our findings are also aligned with binding free energy and RMSD outcomes, thus giving credence to the potential application, and development of these lead molecules as LasR modulating QSIs. The measurement of mean residues and atoms volatility at a receptor's active site over a simulated time is a key determinant of their ability to form stable molecular bonds [81]. Less volatility of atoms at the ligand binding site indicates stronger affinity and binding between the receptor and ligand [82].

The RoG evaluates the levels of folding and compactness of protein–ligand complexes over a simulation time [81]. Here, lower RoG values indicate better thermodynamic orderliness and compactness of ligand atoms and receptor residues, and vice versa. On the other hand, higher RoG values may be linked with unfavourable alterations in protein structure causing varied degrees of folding [83]. This study, the binding of all lead metabolites to LasR did not result in target folding as atoms and residues remained compact and stable through the simulation period (Fig. 7c). Of all metabolites, lonchocarpin (15.58 ± 0.09 Å) had the highest RoG, while azithromycin standard had the higher value (15.59 ± 0.32 Å) when compared to the apo-protein (15.42 ± 0.08 Å). Nonetheless, binding of lonchocarpin to apo-LasR had little impact on its folding. Also, protein folding was observed for the azithromycin-LasR complex at the 70 – 80 ns range (Fig. 7c). Complexes formed by obolactone, cyclocanaliculatin, 5-Hydroxy-7-methoxy-2-phenylchroman-4-one; and 1,4-bis(phenylglyoxaloyl)benzene with LasR had lower RoG values (15.39–15.39 Å) (Supplementary Table S5) suggesting better compactness and thermodynamic orderliness. Again, since RoG values of LasR and bound ligand–protein complexes were closely related or negligible, it further showed that ligand binding had a negligible effect on LasR folding. Thus, *H. annuus* lead phytoconstituents maintained the thermodynamic entropy of LasR. The study of chrysin bound to LasR with a 1.62 nm Rog mean had also been reported to be indicative of ligand structure and system stability [79]. A similar observation of few shifts in the LasR + curcumin system trajectory with Rog maintained between 13.9 and 14.9 Å also indicated system stability [78]. Our RoG observations are partly aligned with the RMSD and RMSF measurements, and point to their ability to form thermodynamically stable complexes with LasR. This supports the potential ability of the 5 lead *H. annuus* metabolites to be developed as stable QS modulators of *P. aeruginosa* LasR. On the other hand, the solvent accessible solvation area (SASA) evaluates changes in protein residue accessibility to near-by solvent molecules. The SASA also determines protein stability and folding, and gives insight into the protein surface area to volume that is exposed and available for interaction with solvent molecules. Hence, a lower SASA is indicative of reduced protein surface area and volume, and which invariably translates to improved stability [84]. Much like the RMSD and RMSF post-dynamic parameters, the unbound LasR, azithromycin-LasR, and 5 lead *H. annuus* metabolites bound to LasR showed stability within the 7600 and 10,200 Å SASA range during the simulation. All lead metabolites showed lower SASA scores, with the exception of lonchocarpin (9034.77 ± 307.81 Å), and compared to higher values recorded for azithromycin (9090.31 Å) and the apo-protein (8923.76 Å). Highest SASA fluctuations were observed from 0 to 45 ns range (Fig. 7d, Supplementary Table S5). Both RoG and SASA outcomes align, indicating stabilization of the folded protein conformation, and confirmed that binding of *H. annuus* lead metabolites to LasR did not cause protein unfolding or expansion. A similar result was observed by Lanrewaju et al. [84] where a decrease in SASA values suggested a good conformational behaviour. Lower SASA values are favourable since higher values indicate protein volume/surface area increase or protein structure expansion which could impact on protein activity [77]. S'thebe et al. [19] also recorded minimal SASA shifts upon the binding of *H. annuus* (Agsun cultivar) seed oil-based phylloquinone, oleic and linoleic acids lead metabolites relative to the standard (azithromycin) upon binding with LasR during a 100 ns simulation run.

In terms of the number of intramolecular hydrogen bonds (IHBs) formed during simulation, fluctuations were fairly stable within the 50–110 range following the binding of lead metabolties to LasR. On average, 1,4-bis(phenylglyoxaloyl)benzene (82) and obolactone (80) complexed with LasR had more IHBs. Cyclocanaliculatin, 5-hydroxy-7-methoxy-2-phenylchroman-4-one, and azithromycin had an average of 79 hydrogen (H) bonds, with the least number of bonds recorded for lonchocarpin (76) (Supplementary Table S5, Supplementary Fig. S5). The relative decrease in hydrogen bonds (H-bonds) upon binding of lonchocarpin, cyclocanaliculatin, 5-Hydroxy-7-methoxy-2-phenylchroman-4-one, and azithromycin to LasR relative to the apo-LasR (average of 81) indicated possible breaks in the formed IHBs. S'thebe et al. [19] also recorded a decrease in IHBs following binding of standard molecules and three lead Agsun essential oil metabolites, relative to apo-LasR. In general, findings indicated that the lead metabolites occupied some intramolecular spaces, while increase in number of IHBs as observed with 1,4-bis(phenylglyoxaloyl)benzene points to higher hydrogen bond interactions being formed between the metabolite complexed with LasR. Values from RMSD align with number of H-bond outcomes, especially for 1,4-bis(phenylglyoxaloyl)benzene and obolactone, suggesting thermodynamic stability and compatibility with LasR. Sadiq et al. [72] had also earlier showed that the maintenance of 2 H-bonds with key LasR amino acid residues (Try56, Thr115) played inalienable roles in stabilizing the complex. Hydrogen bonds have key functions that contribute to stabilizing protein structure. Molecules that demonstrate an ability to form hydrogen bonds have immense potential as drug candidates as they improve drug solubility, while sustaining key precise interactions with their target [75,85].

The stability and binding affinities of complexed systems are inextricably impacted by the type and number of bonds interacting within each system [86]. The observed interactions between the lead *H. annuus* metabolites and LasR over the 100 ns simulation time frame included carbon-hydrogen and conventional H-bonds, van der Waals, alkyl, and pi-alkyl (Fig. 8a–d, Fig. 9a–d, Supplementary Table S4a–b). The simulation interaction depicted as contact maps (residues in contact with

lead ligands forming varied bond interactions) for the top 3 metabolites clearly showed that higher number of total and H-bond interactions, complemented by a high number of hydrophobic interactions contributed to enhance the observed *in silico* AQS activities and free binding energy of the lead metabolites (Fig. 9a–c) relative to azithromycin which had fewer amino acid interactions and an unfavourable bond (Fig. 9d). The total number of bond interactions between complexes at 100 ns for azithromycin-LasR, 1,4-bis(phenylglyoxaloyl)benzene-LasR, obolactone-LasR, cyclocanaliculatin-LasR, 5-hydroxy-7-methoxy-2-phenylchroman-4-one-LasR, and lonchocarpin-LasR systems were 13, 27, 23, 21, 20, and 16, respectively (Supplementary Table S4b). The higher number of interactions and H-bonds, especially in 1,4-bis(phenylglyoxaloyl) benzene, obolactone, and cyclocanaliculatin bound systems correlate well with their lower docking scores and higher negative ΔG_{bind} values. In addition, bond interactions analysis showed 2 (Arg56, Thr110), 3 (Trp55, Asp68, Tyr88), 2 (Thr70, Thr110), and 2 (Thr110, Ala122) conserved H-bond contacts for 1,4-bis(phenylglyoxaloyl)benzene-LasR, obolactone-LasR, 5-hydroxy-7-methoxy-2-phenylchroman-4-one-LasR and cyclocanaliculatin-LasR systems, respectively, compared to none for the azithromycin-LasR system after 100 ns simulation (Supplementary Table S4b). These conserved bonds could also be responsible for the better ΔG_{bind} observed for the metabolites. In contrast to our findings, Sadiq et al. [72] noted that the conserved H-bond interactions of the LasR antagonist, sulfamerazine, with Tyr56,

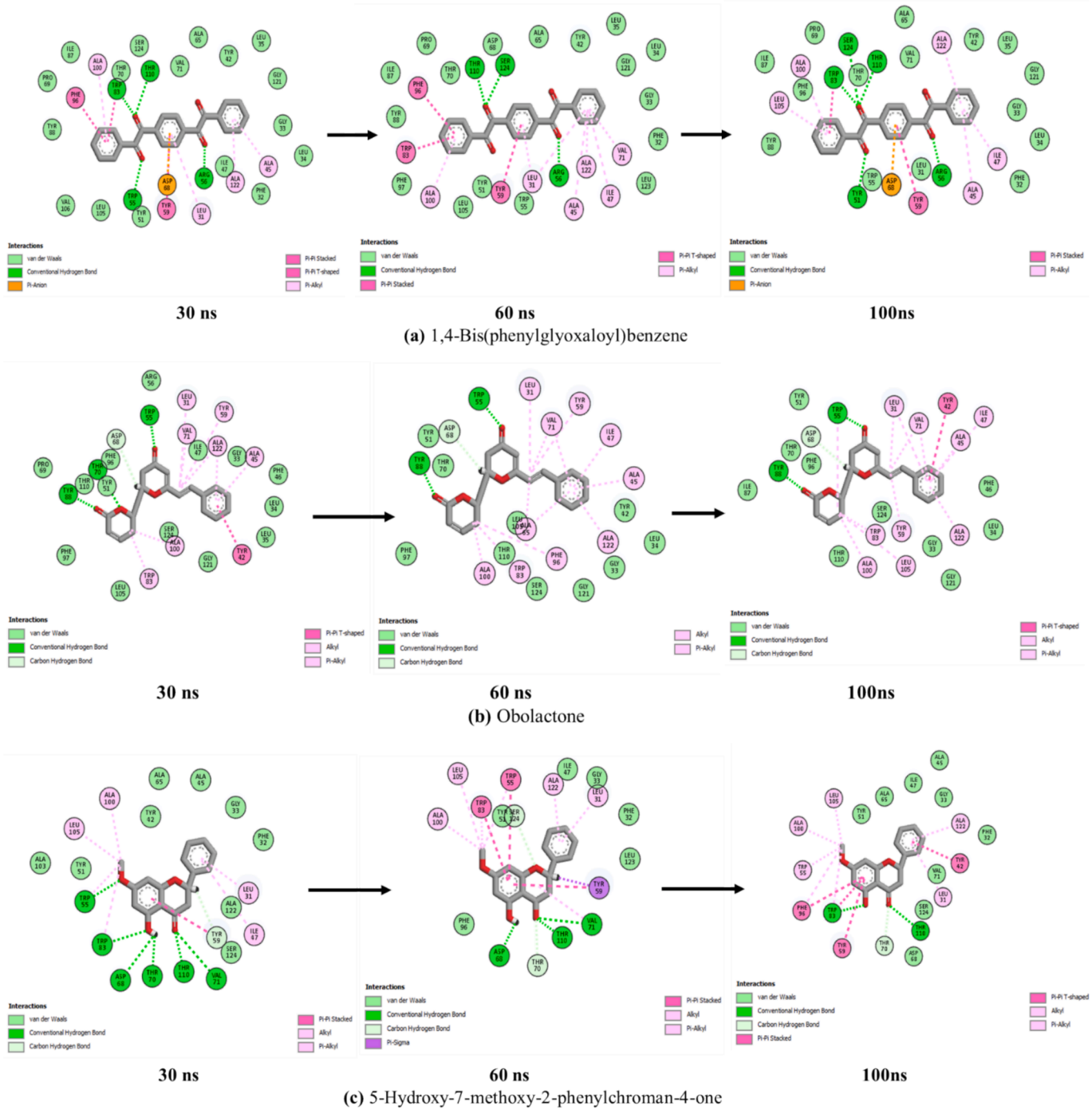

Fig. 8. 2D interaction plots of the 3 lead metabolites and azithromycin standards bound to LasR at 30 ns, 60 ns, and 100 ns simulation. (a) 1,4-Bis(phenylglyoxaloyl) benzene, (b) Obolactone, (c) 5-Hydroxy-7-methoxy-2-phenylchroman-4-one, (d) Azithromycin.

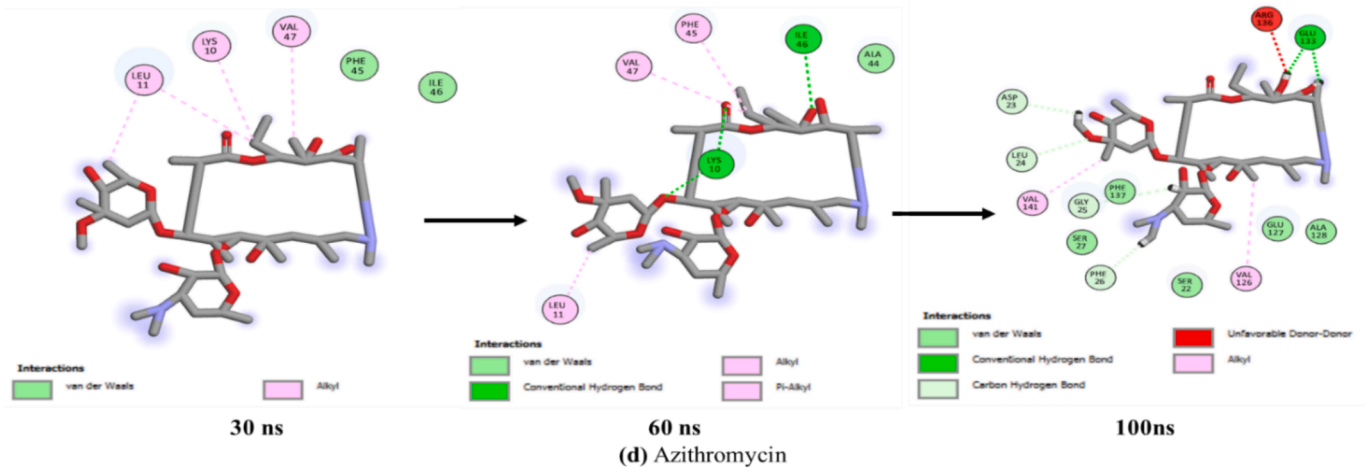

(d) Azithromycin

Fig. 8. (*continued*).

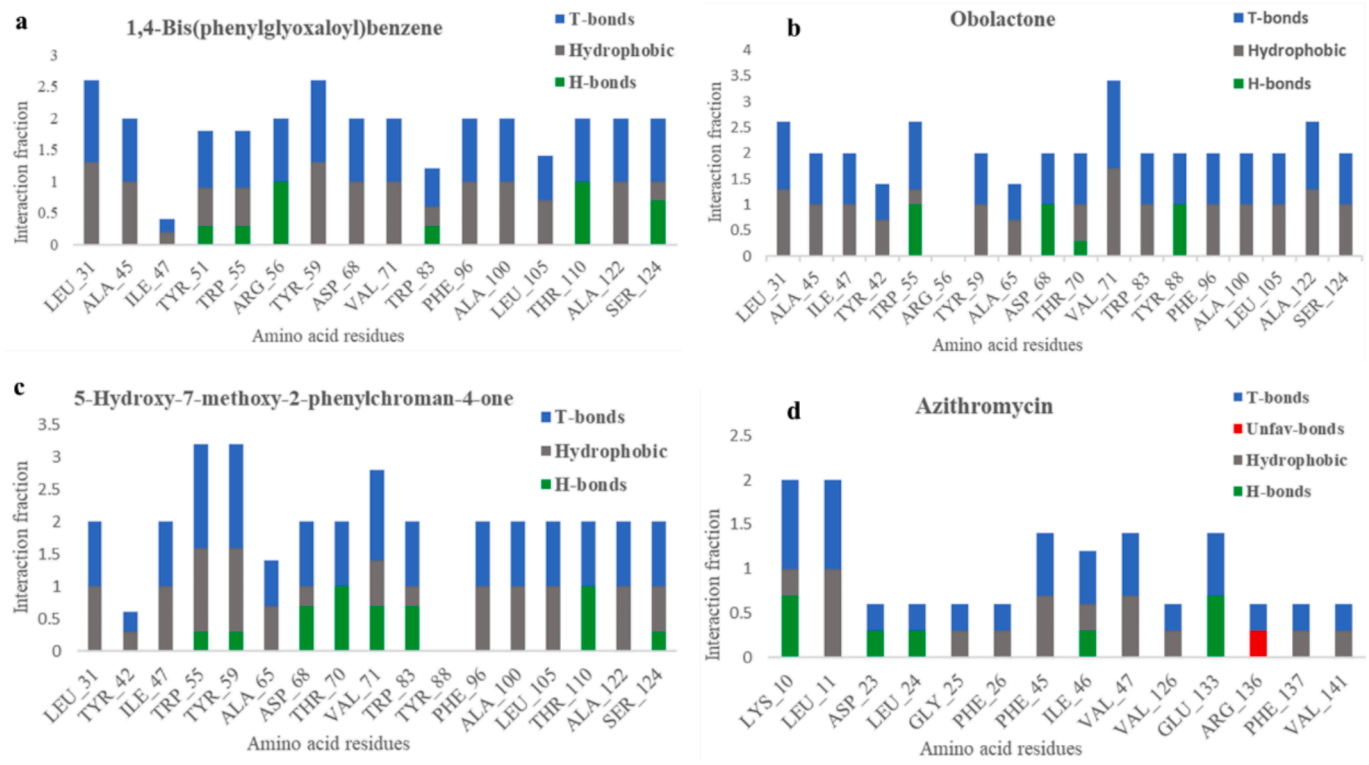

Fig. 9. Protein (amino acid)-ligand contact maps and simulation interaction of the 3 lead metabolites (a) 1,4-Bis(phenylglyoxaloyl)benzene, (b) Obolactone, (c) 5-Hydroxy-7-methoxy-2-phenylchroman-4-one, and (d) Azithromycin.

Trp60, Thr115, and Ser129 were key contributors to the compound's observed ΔG_{bind} (−52.74 kcal/mol) and stability.

The lower number of H-bonds observed for 5-hydroxy-7-methoxy-2-phenylchroman-4-one and lonchocarpin despite their high number of total interactions may have contributed to the lower negative ΔG_{bind} of their bound systems. A similar observation was made by Lanrewaju et al. [87], where total number of interactions did not correlate with ΔG_{bind} for gnetin L bound to VP7C protein. Nevertheless, all the lead *H. annuus* metabolites showed better ΔG_{bind} scores relative to the standards. Again, an unfavourable donor–donor bond was only observed with the azithromycin-LasR system. The reduced stability, docking score and lower negative ΔG_{bind} of the azithromycin-LasR system may be due to the pull exerted by the unfavourable donor–donor bond, and presence of lesser number of interactions and H-bonds [87]. The conserved amino acid residues forming H-bonds after 100 ns simulation of azithromycin, 1,4-bis(phenylglyoxaloyl)benzene, cyclocanaliculatin, obolactone, lonchocarpin, and 5-hydroxy-7-methoxy-2-phenylchroman-4-one complexed with LasR were 0, 2 (Arg56, Thr110), 2 (Thr110, Ala122), 3 (Trp55, Asp68, Tyr88), 1 (Trp55) and 2 (Thr70, Thr110), respectively (Supplementary Table S4b). Again, the most prevalent interactions observed in the top 3 metabolites were hydrophobic and H-bonds, and residues that interact with ligands more than once reflect interaction fractions that exceed 1 (Fig. 9a–d). Obolactone contact with Trp55, Asp68, Tyr88 each had a fraction of 1 (interaction maintained for 100 % of the simulation period). Also, contact of 1,4-bis(phenylglyoxaloyl)benzene (0.7, 70 %) and 5-hydroxy-7-methoxy-2-phenylchroman-4-one (0.3, 30 %) with Ser124, and 100 % contact maintained with Thr110 for both metabolites were key to stabilizing both bound systems. These

metabolites formed H-bond with Trp55, while only obolactone maintained a H-bond with Tyr88 for 100 % of the simulation period. Earlier studies had also shown that H- or hydrophobic-bond contacts with hydrophobic pocket residues are key to stabilizing and ensuring the function of QSIs [88,89]. The Tyr88 residues is also a key conserved residue with atoms tightly linked to the ligand binding (R binder) pocket of LasR [90]. This may have also contributed to the highest negative ΔG_{bind} observed for the obolactone-LasR system relative to other metabolites. Furthermore, interaction of metabolites with conserved Thr75 and Asp 73 (Supplementary Table S3, Fig. S1) has been reported to favourably mediate the packing of LasR alpha 3, 4 and 5 folds (helices) unto the centralized beta-sheet, ensuring correct LasR hydrophobic centre formation. This interaction-induced protein folding attribute is key to stabilizing the protein, and in selecting ligands with potential QSI activity [90]. Overall, higher total number of interactions and hydrogen bond counts contribute to improve target inhibition and correspond to prolonged residency of modulators or inhibitors at the target catalytic site, thereby enhancing modulatory activity [80]. The high number of H-bond interactions, as well as alkyl, and pi-alkyl interactions maintained between *H. annuus* metabolites and LasR contributed to the thermodynamic stability and binding affinity of their systems [80]. These *in silico* outcomes showed as high binding free energies and strong bond interactions, thermodynamic stability and compactness of bound lead ligand-LasR systems, particularly in the order 1,4-bis(phenylglyoxaloyl) benzene > obolactone > 5-hydroxy-7-methoxy-2-phenylchroman-4-one, indicated the lead metabolites potential AQS and modulatory effects against *P. aeruginosa* LasR. Future studies could transit to added validation of findings using *in vivo* techniques after further derivatization or modification of the leads to enhance their function as potential QSIs [91].

4. Conclusion

Overall, our *in vitro* and *in silico* metabolomic and cheminformatic bioprospection of six *H. annuus* Pannar seed cultivars, their extracts and metabolites, provided evidence of the quorum sensing (QS) modulatory properties of the seed extracts and metabolites against *P. aeruginosa* LasR system. The PAN 7102 cultivar extracts showed the best antibacterial, anti-biofilm and AQS activities. Furthermore, metabolomic analysis of the cultivars identified several metabolites for the first time. These metabolites include methoxymellein, hydroxytetradecanedioic acid, koninginin G, geoside, pinellic acid, and methylpicraquassioside A. Chemometric PCA and PLS-DA analyses showed distinct metabolomic signatures and variance which were largely driven by aqueous and ethanolic extracts of Pannar cultivars 7102, 7160, and 7156. Subsequent *in silico* bioprospection and validation showed that obolactone, 5-hydroxy-7-methoxy-2-phenylchroman-4-one and 1,4-bis(phenylglyoxaloyl)benzene had the best AQS activity against the *P. aeruginosa* LasR. For the first time, this study demonstrated that sunflower, Pannar seed extracts and their lead compounds had significant AQS activities. Also, all lead metabolites [obolactone, 5-hydroxy-7-methoxy-2-phenylchroman-4-one, 1,4-bis(phenylglyoxaloyl)benzene, cyclocanaliculatin, lonchocarpin] showed good pharmacokinetic and drug-like properties, given their conformation to the Lipinski rule of 5. Thus, these leads have the potential to be developed into oral QSIs which could be efficacious as modulators of LasR and QS-related virulence factors (motility, cell attachment, biofilm, violacein and pyocyanin expression) to mitigate *P. aeruginosa* infections pathogenicity. Nonetheless, further exploration through in-depth *in vivo* and derivatization studies to evaluate the toxicity profile of the lead metabolites and their modified derivatives is required prior to use in various therapeutic formulations targeting LasR modulation.

CRediT authorship contribution statement

Akshay Raghoonanadan: Validation, Methodology, Investigation, Formal analysis. **Yamkela Dweba:** Visualization, Investigation, Formal analysis. **Christiana E. Aruwa:** Co-Supervision, Writing – original draft, review & editing. **Saheed Sabiu:** Writing – review & editing, Supervision, Project administration, Funding acquisition, Conceptualization.

Funding

This work was supported in part by the Directorate of Research and Postgraduate Support, Durban University of Technology (DUT); the South African Medical Research Council (SAMRC) through a Self-Initiated Research Grant, as well as the South African National Research Foundation (NRF) Competitive Programme for Rated Researchers Support (SRUG2204193723) and the International Centre for Genetic Engineering and Biotechnology (ICGEB) (Grant No. ZAF/HDI/CRP/024) awarded to S. Sabiu. It is important to note that the views and opinions expressed in this work are those of the authors and do not necessarily reflect the official views of the funding agencies.

Declaration of competing interest

The authors declare that they have no known competing financial interests or personal relationships that could have appeared to influence the work reported in this paper.

Acknowledgements

The authors acknowledge the Directorate of Research and Postgraduate Support, Durban University of Technology, South Africa. We also acknowledge the Department of Science and Technology Innovation (DSTI) supported Centre for High Performance Computing (CHPC) cyber-infrastructure ('HEAL1361' cluster-specific resident program) for the access to cluster for MD simulations.

Appendix A. Supplementary material

Supplementary data to this article can be found online at https://doi.org/10.1016/j.bioorg.2024.108046.

Data availability

Data will be made available on request.

References

[1] K.W.K. Tang, B.C. Millar, J.E. Moore, Antimicrobial resistance (AMR), Br. J. Biomed. Sci. 80 (2023) 11387, https://doi.org/10.3389/bjbs.2023.11387.
[2] M. Ferri, E. Ranucci, P. Romagnoli, V. Giaccone, Antimicrobial resistance: a global emerging threat to public health systems, Crit. Rev. Food Sci. Nutr. 57 (2017) 2857–2876, https://doi.org/10.1080/10408398.2015.1077192.
[3] P. Dadgostar, Antimicrobial resistance: implications and costs, Infect. Drug Resist. 12 (2019) 3903–3910, https://doi.org/10.2147/IDR.S234610.
[4] F. Prestinaci, P. Pezzotti, A. Pantosti, Antimicrobial resistance: a global multifaceted phenomenon, Pathog. Glob. Health 109 (2015) 309–318, https://doi.org/10.1179/2047773215Y.0000000030.
[5] Food and Drugs Administration, FDA updates warnings for fluoroquinolone antibiotics on risks of mental health and low blood sugar adverse reaction, https://www.fda.gov/news-events/press-announcements/fdaupdates-warnings fluoroquinolone-antibiotics-risks-mental-health-and-low-bloodsugar-adverse, 2018 (accessed 4 January 2024).
[6] South African Antimicrobial Resistance National Strategy Framework 2017 – 2024, A One Health Approach. https://knowledgehub.health.gov.za/elibrary/south-african-antimicrobial-resistance-national-strategy-framework-one-health-approach, 2017 (accessed 12 March 2024).
[7] S.Y. Essack, C. Connolly, A.W. Sturm, Antibiotic use and resistance in public-sector hospitals in KwaZulu-Natal, South Afr. Med. J. 95 (2005) 865–870. https://journals.co.za/doi/pdf/10.10520/EJC68368.
[8] J. Lin, J. Cheng, Quorum sensing in *Pseudomonas aeruginosa* and its relationship to biofilm development, in: N.K. Rathinam, R.K. Sani (Eds.), Introduction to Biofilm Engineering, American Chemical Society, Washington, DC, 2019, pp. 1–16.
[9] S.T. Rutherford, B.L. Bassler, Bacterial quorum sensing: Its role in virulence and possibilities for its control, Cold Spring Harb. Perspect. Med. 2 (2012) a012427, https://doi.org/10.1101/cshperspect.a012427.

[10] G. Mancuso, A. Midiri, E. Gerace, C. Biondo, Bacterial antibiotic resistance: the most critical pathogens, Pathogens 10 (2021) 1310, https://doi.org/10.3390/pathogens10101310.
[11] F. Brindhadevi, F. Lewisoscar, E. Mylonakis, S. Shanmugam, T.N. Verma, A. Pugazhendhi, Biofilm and quorum sensing mediated pathogenicity in *Pseudomonas aeruginosa*, Process Biochem. 96 (2020) 49–57, https://doi.org/10.1016/j.procbio.2020.06.001.
[12] D.M.P. De Oliveira, B.M. Forde, T.J. Kidd, P.N. Harris, M.A. Schembri, S. A. Beatson, D.L. Paterson, M.J. Walker, Antimicrobial resistance in ESKAPE pathogens, Clin. Microbiol. Rev. 33 (2020) e00181-19, https://doi.org/10.1128/cmr.00181-19.
[13] Y.M. Chong, K.Y. How, W.F. Yin, K.G. Chan, The effects of Chinese herbal medicines on the quorum sensing-regulated virulence in *Pseudomonas aeruginosa* PAO1, Molecules 23 (2018), https://doi.org/10.3390/molecules23040972.
[14] C. Om, F. Daily, E. Vlieghe, J.C. Mclaughlin, M.L. Mclaws, If it's a broad spectrum, it can shoot better: Inappropriate antibiotic prescribing in Cambodia, Antimicrob. Resist. Infect. Control. 5 (2016) 1–8, https://doi.org/10.1186/s13756-016-0159-7.
[15] S. Guo, Y. Ge, K.N. Jom, A review of phytochemistry, metabolite changes, and medicinal uses of the common sunflower seed and sprouts (*Helianthus annuus* L.), Chem. Cent. J. 11 (2017) 1–10, https://doi.org/10.1186/s13065-017-0328-7.
[16] A.F. Muhammad, M. Nadeem, K.M. Issa, S. Hussain, Nutritional and therapeutic potential of sunflower seeds: a review, Br. Food J. 114 (2012) 544–552, https://doi.org/10.1108/00070701211219559.
[17] S. Rauf, R. Ortiz, M. Shehzad, W. Haider, I. Ahmed, The exploitation of sunflower (*Helianthus annuus* L.) seed and other parts for human nutrition, medicine and the industry, Helia 43 (2020) 167–184, https://doi.org/10.1515/helia-2020-0019.
[18] O.A. Adeleye, M.N. Femi-Oyewo, O.A. Bamiro, L.G. Bakre, A. Alabi, J.S. Ashidi, O. A. Balogun-Agbaje, O.M. Hassan, G. Fakoya, Ethnomedicinal herbs in African traditional medicine with potential activity for the prevention, treatment, and management of coronavirus disease, Fut. J. Pharm. Sci. 7 (2021) (2019) 1–14, https://doi.org/10.1186/s43094-021-00223-5.
[19] N.W. S'thebe, J.O. Aribisala, S. Sabiu, Cheminformatics bioprospection of sunflower seeds' oils against quorum sensing system of *Pseudomonas aeruginosa*, Antibiotics 12 (2023) 504, https://doi.org/10.3390/antibiotics12030504.
[20] C.E. Aruwa, S. Amoo, T. Kudanga, Phenolic compound profile and biological activities of Southern African *Opuntia ficus-indica* fruit pulp and peels, LWT 111 (2019) 337–344, https://doi.org/10.1016/j.lwt.2019.05.028.
[21] W.P. Shi, H. Zeng, C.X. Wan, Z.B. Zhou, Amicoumacins from a desert bacterium: quorum sensing inhibitor against *Chromobacterium violaceum*, Nat. Prod. Res. 35 (2021) 5508–5512, https://doi.org/10.1080/14786419.2020.1788554.
[22] T. Köhler, G.G. Perron, A. Buckling, C. Van Delden, Quorum sensing inhibition selects for virulence and cooperation in *Pseudomonas aeruginosa*, PLoS Pathog. 6 (2010) e1000883, https://doi.org/10.1371/journal.ppat.1000883.
[23] A. Sen, A. Batra, Evaluation of antimicrobial activity of different solvent extracts of medicinal plant: *Melia azedarach* L, Int. J. Curr. Pharm. Res. 4 (2013) 67–73. https://www.innovareacademics.in/journal/ijcpr/Issues/Vol4Issue2/488.pdf.
[24] V. Kuete, B. Ngameni, C.C. Fotso Simo, T.R. Kengap, N.B. Tchaleu, J.J.M. Meyer, N. Lall, J.R. Kuiate, Antimicrobial activity of the crude extracts and compounds from *Ficus chlamydocarpa* and *Ficus cordata* (Moraceae), J. Ethnopharmacol. 120 (2008) 17–24, https://doi.org/10.1016/j.jep.2008.07.026.
[25] Clinical and Laboratory Standards Institute, Methods for dilution antimicrobial susceptibility tests for bacteria that grow aerobically (Approved standard M07). https://clsi.org/media/1928/m07ed11_sample.pdf, 2018 (accessed 23 May 2024).
[26] H.Y. Chenia, Anti-quorum sensing potential of crude *Kigelia africana* fruit extracts, Sensors 13 (2013) 2802–2817, https://doi.org/10.3390/s130302802.
[27] N.M. Seleem, H.K. Abd El Latif, M.A. Shaldam, A. El-Ganiny, Drugs with new lease of life as quorum sensing inhibitors for combating MDR *Acinetobacter baumannii* infections, Eur. J. Clin. Microbiol. Infect. Dis. 39 (2020) 1687–1702, https://doi.org/10.1007/s10096-020-03882-z.
[28] S. Bahari, H. Zeighami, H. Mirshahabi, S. Roudashti, F. Haghi, Inhibition of *Pseudomonas aeruginosa* quorum sensing by subinhibitory concentrations of curcumin with gentamicin and azithromycin, J. Glob. Antimicrob. Resist. 10 (2017) 21–28, https://doi.org/10.1016/j.jgar.2017.03.006.
[29] D.G. Ha, S.L. Kuchma, G.A. O'Toole, Plate-based assay for swimming motility in *Pseudomonas aeruginosa*, Methods Mol Biol. 1149 (2014) 59–65, https://doi.org/10.1007/978-1-4939-0473-0_7.
[30] I.T. Baloyi, S. Cosa, S. Combrinck, C.M. Leonard, A.M. Viljoen, Anti-quorum sensing and antimicrobial activities of South African medicinal plants against uropathogens, South Afr. J. Bot. 122 (2019) 484–491. http://hdl.handle.net/2263/68605.
[31] I.M. Famuyide, A.O. Aro, F.O. Fasina, J.N. Eloff, L.J. McGaw, Antibacterial and antibiofilm activity of acetone leaf extracts of nine under-investigated South African *Eugenia* and *Syzygium* (Myrtaceae) species and their selectivity indices, BMC Complement Altern. Med. 19 (2019) 1–13, https://doi.org/10.1186/s12906-019-2547-z.
[32] C.L. Quave, M. Estévez-Carmona, C.M. Compadre, G. Hobby, H. Hendrickson, K. E. Beenken, M.S. Smeltzer, Ellagic acid derivatives from *Rubus ulmifolius* inhibit *Staphylococcus aureus* biofilm formation and improve response to antibiotics, PLoS One 7 (2012) e28737, https://doi.org/10.1371/journal.pone.0028737.
[33] A. Rougereau, A. Guiller, J. Gore, O. Person, Determination of fat–soluble vitamins by HPLC, in: W. Baltes, P.B. Czedik-Eysenbery, W. Pfannhauser (Eds.), Recent Development in Food Analysis, Euro Food Chem I, Austria, 1982, pp. 17–20.
[34] Z. Pang, Y. Lu, G. Zhou, F. Hui, L. Xu, C. Viau, A. Spigelman, P. MacDonald, D. Wishart, S. Li, J. Xia, MetaboAnalyst 6.0: towards a unified platform for metabolomics data processing, analysis and interpretation, Nucleic Acids Res. 52 (2024) W398–W406, https://doi.org/10.1093/nar/gkae253.
[35] E.F. Pettersen, T.D. Goddard, C.C. Huang, G.S. Couch, D.M. Greenblatt, E.C. Meng, T.E. Ferrin, UCSF Chimera—a visualization system for exploratory research and analysis, J. Comput. Chem. 25 (2004) 1605–1612, https://doi.org/10.1002/jcc.20084.
[36] A. Chiorcea-Paquim, T.A. Enache, E. De Souza Gil, A.M. Oliveira-Brett, Natural phenolic antioxidants electrochemistry: towards a new food science methodology, Compr. Rev. Food Sci. Food Saf. 19 (2020) 1680–1726, https://doi.org/10.1111/1541-4337.12566.
[37] H.G. Gowtham, M. Murali, S.B. Singh, C. Shivamallu, S. Pradeep, C.S. Shivakumar, S. Anandan, A. Thampy, R.R. Achar, E. Silina, V. Stupin, J. Ortega-Castro, J. Frau, D. Glossman-Mitnik, Phytoconstituents of *Withania somnifera* unveiled ashwagandhanolide as a potential drug targeting breast cancer: investigations through computational, molecular docking and conceptual DFT studies, PLoS One 17 (2022) e0275432, https://doi.org/10.1371/journal.pone.0275432.
[38] E. Afgan, D. Baker, B. Batut, M. Van Den Beek, D. Bouvier, M. Čech, J. Chilton, D. Clements, N. Coraor, B.A. Grüning, A. Guerler, The Galaxy platform for accessible, reproducible and collaborative biomedical analyses: 2018 update, Nucleic Acids Res. 46 (2018) (2018) W537–W544.
[39] A. Daina, O. Michielin, V. Zoete, SwissADME: a free web tool to evaluate pharmacokinetics, drug-likeness and medicinal chemistry friendliness of small molecules, Sci. Rep. 7 (2017) 1–13, https://doi.org/10.1038/srep42717.
[40] P. Gonnet, P-SHAKE: a quadratically convergent SHAKE in O(n2), J. Comput. Phys. 220 (2007) 740–750, https://doi.org/10.1016/j.jcp.2006.05.032.
[41] M. Ylilauri, O.T. Pentikäinen, MMGBSA As a tool to understand the binding affinities of filamin–peptide interactions, J. Chem. Inf. Model. 53 (2013) 2626–2633, https://doi.org/10.1021/ci4002475.
[42] BIOVIA, Discovery Studio Visualizer. v21.1.0.20298, Dassault Systèmes, San Diego, CA, USA, Dassault Systèmes, 2021.
[43] E. Seifert, OriginPro 9.1: scientific data analysis and graphing software-software review, J. Chem. Inf. Model. 54 (2014) 1552, https://doi.org/10.1021/ci500161d.
[44] J.F. Fatriansyah, A.G. Boanerges, S.R. Kurnianto, A.F. Pradana, F. Fadilah, S. N. Surip, Molecular dynamics simulation of ligands from *Anredera cordifolia* (Binahong) to the main protease (Mpro) of SARS-CoV-2, J. Trop. Med. 2022 (1) (2022) 1178228.
[45] Clinical and Laboratory Standards Institute, Performance standards for antimicrobial susceptibility testing (CLSI supplement M100S), https://clsi.org/standards/products/microbiology/documents/m100/, 2020 (accessed 23 May 2024).
[46] M. Sisay, N. Bussa, T. Gashaw, G. Mengistu, Investigating *in vitro* antibacterial activities of medicinal plants having folkloric repute in Ethiopian Traditional Medicine, 2515690X19886276, J. Evid-Based Integ. Med. 24 (2019), https://doi.org/10.1177/2515690X19886276.
[47] C. de Torres, M.C. Díaz-Marotoa, I. Hermosín-Gutiérrez, M.S. Pérez-Coelloa, Effect of freeze-drying and oven-drying on volatiles and phenolics composition of grape skin, Anal. Chim. Acta 660 (2010) 177–182. 10.1016/j.aca.2009.10.005.
[48] M.A. Aboki, M. Mohammed, S.H. Musa, B.S. Zuru, H.M. Aliyu, M. Gero, I.M. Alibe, B. Inuwa, Physicochemical and anti-microbial properties of sunflower (*Helianthus annuus* L.) seed oil, Int. J. Sci. Technol. 2 (2012) 151–154.
[49] R. Puttha, K. Venkatachalam, S. Hanpakdeesakul, J. Wongsa, T. Parametthanuwat, P. Srean, K. Pakeechai, N. Charoenphun, Exploring the potential of sunflowers: agronomy, applications, and opportunities within bio-circular-green economy, Horticulturae 9 (2023) 1079, https://doi.org/10.3390/horticulturae9101079.
[50] G. Nemer, N. Louka, P. Rabiller Blandin, R.G. Maroun, E. Vorobiev, T. Rossignol, J.-M. Nicaud, E. Guénin, M. Koubaa, Purification of natural pigments violacein and deoxyviolacein produced by fermentation using *Yarrowia lipolytica*, Molecules 28 (2023) 4292, https://doi.org/10.3390/molecules28114292.
[51] S. Sasidharan, Y. Chen, D. Saravanan, K. Sundram, L.Y. Latha, Extraction, isolation and characterization of bioactive compounds from plants' extracts, Afr. J. Tradit. Complement. Altern. Med. 8 (2011) (2011) 1–10, https://doi.org/10.4314/ajtcam.v8i1.60483.
[52] M. Konzen, D.D. Marco, C.A.S. Cordova, T.O. Vieira, R.G. Antonio, T.B. Creczynski-Pasa, Antioxidant properties of violacein: possible relation on its biological function, Bioorg. Med. Chem. 14 (2006) 8307–8313, https://doi.org/10.1016/j.bmc.2006.09.013.
[53] M. Venkatramanan, P. Sankar Ganesh, R. Senthil, J. Akshay, A. Veera Ravi, K. Langeswaran, J. Vadivelu, S. Nagarajan, K. Rajendran, E.M. Shankar, Inhibition of quorum sensing and biofilm formation in *Chromobacterium violaceum* by fruit extracts of *Passiflora edulis*, ACS, Omega 5 (2020) 25605–25616, https://doi.org/10.1021/acsomega.0c02483.
[54] C.F. de Brito, C.B. Carvalho, F. Santos, R.T. Gazzinelli, S.C. Oliveira, V. Azevedo, S. M. Teixeira, *Chromobacterium violaceum* genome: molecular mechanisms associated with pathogenicity, Genet. Mol. Res. 3 (2004) 148–161. https://pubmed.ncbi.nlm.nih.gov/15100995/.
[55] R. Roy, M. Tiwari, G. Donelli, V. Tiwari, Strategies for combating bacterial biofilms: a focus on anti-biofilm agents and their mechanisms of action, Virulence 9 (2018) 522–554, https://doi.org/10.1080/21505594.2017.1313372.
[56] M.R. Walmiki, R.V. Ravishankar, Cell attachment inhibition and anti-biofilm activity of *Syzygium aromaticum*, *Cuminum cyminum* and *Piper nigrum* essential oils against pathogenic bacteria, J. Essent. Oil-Bear. Plants. 20 (2017) 59–68, https://doi.org/10.1080/0972060X.2017.1287011.
[57] J.F. Parsons, B.T. Greenhagen, K. Shi, K. Calabrese, H. Robinson, J.E. Ladner, Structural and functional analysis of the pyocyanin biosynthetic protein PhzM from *Pseudomonas aeruginosa*, Biochemistry 46 (2007) 1821–1828, https://doi.org/10.1021/bi6024403.
[58] R. Fan, C. Peng, X. Zhang, D. Qiu, G. Mao, Y. Lu, J. Zeng, A comparative UPLC-Q-Orbitrap-MS untargeted metabolomics investigation of different parts of *Clausena*

lansium (Lour.) skeels, Food Sci. Nutr. 8 (2020) 5811–5822, https://doi.org/10.1002/fsn3.1841.
[59] S.A. Skubel, X. Su, A. Poulev, L.C. Foxcroft, V. Dushenkov, I. Raskin, Metabolomic differences between invasive alien plants from native and invaded habitats, Sci. Rep. 10 (2020) 9749, https://doi.org/10.1038/s41598-020-66477-w.
[60] K.L. Mikolajczak, C.R. Smith, I.A. Wolff, Phenolic and sugar components of Armavireo variety sunflower (*Helianthus annuus*) seed meal, J. Agric. Food Chem. 18 (1970) 27–32, https://doi.org/10.1021/jf60167a026.
[61] A. Poulev, J.M. O'Neal, S. Logendra, R.B. Pouleva, V. Timeva, A.S. Garvey, D. Gleba, I.S. Jenkins, B.T. Halpern, R. Kneer, G.M. Cragg, Elicitation, a new window into plant chemodiversity and phytochemical drug discovery, J. Med. Chem. 46 (2003) 2542–2547, https://doi.org/10.1021/jm020359t.
[62] A. Dalal, T. Kushwaha, G. Choudhir, K.K. Inampudi, T. Karmakar, P. Hariprasad, S. L. Gholap, Computational investigations on the potential role of hygrophorones as quorum sensing inhibitors against LasR protein of *Pseudomonas aeruginosa*, J. Biomol. Struct. Dyn. 41 (2023) 249–2259.
[63] M. Shoaib, Y. Ali, Y. Shen, J. Ni, Identification of potential natural products derived from fungus growing termite, inhibiting *Pseudomonas aeruginosa* quorum sensing protein LasR using molecular docking and molecular dynamics simulation approach, J. Biomol. Struct. Dyn. 42 (2024) 1126–1144.
[64] G. Chen, A.J. Seukep, M. Guo, Recent advances in molecular docking for the research and discovery of potential marine drugs, Mar. Drugs 18 (2020) 545, https://doi.org/10.3390/md18110545.
[65] Z. Cai, M. Zafferani, O.M. Akande, A.E. Hargrove, Quantitative structure–activity relationship (QSAR) study predicts small-molecule binding to RNA structure, J. Med. Chem. 65 (2022) 7262–7277, https://doi.org/10.1021/acs.jmedchem.2c00254.
[66] D.R. Koes, C.J. Camacho, ZINCPharmer: pharmacophore search of the ZINC database, Nucleic Acids Res. 40 (2012) W409–W414, https://doi.org/10.1093/nar/gks378.
[67] J.A. Arnott, S.L. Planey, The influence of lipophilicity in drug discovery and design, Expert Opin. Drug Discov. 7 (2012) 863–875, https://doi.org/10.1517/17460441.2012.714363.
[68] K. Palm, P. Stenberg, K. Luthman, P. Artursson, Polar molecular surface properties predict the intestinal absorption of drugs in humans, Pharm. Res. 14 (1997) 568–571, https://doi.org/10.1023/a:1012188625088.
[69] C.A. Lipinski, Lead-and drug-like compounds: the rule-of-five revolution, Drug Discov. Today Technol. 1 (2004) 337–341, https://doi.org/10.1016/j.ddtec.2004.11.007.
[70] D.F. Veber, S.R. Johnson, H.Y. Cheng, B.R. Smith, K.W. Ward, K.D. Kopple, Molecular properties that influence the oral bioavailability of drug candidates, J. Med. Chem. 45 (2002) 2615–2623, https://doi.org/10.1021/jm020017n.
[71] S. Sabiu, F.O. Balogun, S.O. Amoo, Phenolics profiling of *Carpobrotus edulis* (L.) N. E.Br. and Insights into molecular dynamics of their significance in type 2 diabetes therapy and its retinopathy complication, Molecules 26 (2021) 4867, https://doi.org/10.3390/molecules26164867.
[72] S. Sadiq, N.F. Rana, M.A. Zahid, M.K. Zargaham, T. Tanweer, A. Batool, A. Naeem, A. Nawaz, Z. Muneer, A.R. Siddiqi, Virtual screening of FDA-approved drugs against LasR of *Pseudomonas aeruginosa* for antibiofilm potential, Molecules 25 (2020) 3723.
[73] J.O. Aribisala, S. Sabiu, Cheminformatics identification of phenolics as modulators of penicillin-binding protein 2a of *Staphylococcus aureus*: a structure–activity-relationship-based study, Pharmaceutics 14 (2022) 1818, https://doi.org/10.3390/pharmaceutics14091818.
[74] D. Ramirex, J. Caballero, Is it reliable to use common molecular docking methods for comparing the binding affinities of enantiomer pairs for their protein target? Int. J. Mol. Sci. 17 (2016) 525, https://doi.org/10.3390/ijms17040525.
[75] X. Du, Y. Li, Y.L. Xia, S.M. Ai, J. Liang, P. Sang, X.L. Ji, S.Q. Liu, Insights into protein–ligand interactions: mechanisms, models, and methods, Int. J. Mol. Sci. 17 (2016) 144, https://doi.org/10.3390/ijms17020144.
[76] L.H.F.D. de Lima, M.L. Fernandez-Quintéro, R.E.O. Rocha, D.C.B. Mariano, R.C. de Melo-Minardi, K.R. Liedl, Conformational flexibility correlates with glucose tolerance for point mutations in β-glucosidases–a computational study, J. Biomol. Struct. Dyn. 39 (2021) 1621–1634, https://doi.org/10.1080/07391102.2020.1734484.
[77] S.S. Mousavi, A. Karami, T.M. Haghighi, S.G. Tumilaar, R. Fatimawali, R. Idroes, S. Mahmud, I. Celik, D. Ağagündüz, T.E. Tallei, T.B. Emran, *In silico* evaluation of Iranian medicinal plant phytoconstituents as inhibitors against main protease and the receptor-binding domain of SARS-CoV-2, Molecules 26 (2021) 5724, https://doi.org/10.3390/molecules26185724.
[78] L.M. Molina, D.C.A. Naravaez, M.V.P. Morocho, Z.M.R. Vazquez, A. Pérez, M. L. Hurtado-León, C. Lossada, L. González-Paz, Interaction of phytochemicals with proteins associated with mucopolysaccharide biosynthesis in *Pseudomonas aeruginosa*: a predictive study of biomedical interest, Biointer. Res. Appl. Chem. 14 (2024) 1–13.
[79] A.F. Lal, P.S. Gupta, P.K. Yadav, *In silico* study of phenol explorer database as potential inhibitors of quorum-sensing regulated pathogenicity in *Pseudomonas aeruginosa*, Biomed. Pharmacol. J. 16 (2023) 1577–1590.
[80] R.E. Rocha, E.J. Chaves, P.H. Fischer, L.S. Costa, I.B. Grillo, L.E. da Cruz, F. C. Guedes, C.H. da Silveira, M.T. Scotti, A.D. Camargo, A higher flexibility at the SARS-CoV-2 main protease active site compared to SARS-CoV and its potentialities for new inhibitor virtual screening targeting multi-conformers, J. Biomol. Struct. Dyn. 182 (2021) 1–21, https://doi.org/10.1080/07391102.2021.1924271.
[81] M.H. Baig, D.R. Sudhakar, P. Kalaiarasan, N. Subbarao, G. Wadhawa, M. Lohani, M.K.A. Khan, A.U. Khan, Insight into the effect of inhibitor resistant s130g mutant on physico-chemical properties of SHV type betalactamase: a molecular dynamics study, PLoS One 9 (2014) e11245, https://doi.org/10.1371/journal.pone.0112456.
[82] J.O. Aribisala, K. Idowu, T.R. Makhanya, S. Sabiu, Cheminformatics identification of phenolics as modulators of key penicillin—binding proteins of *Escherichia coli* towards interventive antibacterial therapy, Mol. Simul. 2023 (2023) 1–17, https://doi.org/10.1080/08927022.2023.2228423.
[83] M.Y. Lobanov, N.S. Bogatyreva, O.V. Galzitskaya, Radius of gyration as an indicator of protein structure compactness, Mol. Biol. 42 (2008) 623–628, https://doi.org/10.1134/S0026893308040195.
[84] A.A. Lanrewaju, A.M. Enitan-Folami, M.M. Nyaga, S. Sabiu, F.M. Swalaha, Metabolites profiling and cheminformatics bioprospection of selected medicinal plants against the main protease and RNA-dependent RNA polymerase of SARS-CoV-2, J. Biomol. Struct. Dyn. 2023 (2023) 1–21, https://doi.org/10.1080/07391102.2023.2236718.
[85] B. Kuhn, P. Mohr, M. Stahl, Intramolecular hydrogen bonding in medicinal chemistry, J. Med. Chem. 53 (2010) 2601–2611, https://doi.org/10.1021/jm100087s.
[86] M. Murali, F. Ahmed, H.G. Gowtham, J.O. Aribisala, R.A. Abdulsalam, A.A. Shati, M.Y. Alfaifi, R.Z. Sayyed, S. Sabiu, K.N. Amruthesh, Exploration of CviR-mediated quorum sensing inhibitors from *Cladosporium* spp. against *Chromobacterium violaceum* through computational studies, Sci. Rep. 13 (2023) 15505, https://doi.org/10.1038/s41598-023-42833-4.
[87] A.A. Lanrewaju, A.M. Enitan-Folami, S. Sabiu, F.M. Swalaha, Computational bioprospection of selected plant secondary metabolites against VP7 (capsid protein) of rotavirus A, Sci. African. 23 (2024) e02109, https://doi.org/10.1016/j.sciaf.2024.e02109.
[88] A.R. McCready, J.E. Paczkowski, B.R. Henke, B.L. Bassler, Structural determinants driving homoserine lactone ligand selection in the *Pseudomonas aeruginosa* LasR quorum-sensing receptor, Proc. Natl. Acad. Sci. USA 116 (2019) 245–254.
[89] L. Zhong, V. Ravichandran, N. Zhang, H. Wang, X. Bian, Y. Zhang, A. Li, Attenuation of *Pseudomonas aeruginosa* quorum sensing by natural products: Virtual screening, evaluation and biomolecular interactions, Int. J. Mole. Sci. 21 (2020) 2190.
[90] M.J. Bottomley, E. Muraglia, R. Bazzo, A. Carfì, Molecular insights into quorum sensing in the human pathogen *Pseudomonas aeruginosa* from the structure of the virulence regulator LasR bound to its autoinducer, J. Biol. Chem. 282 (2007) 13592–13600, https://doi.org/10.1074/jbc.M700556200.
[91] C. Lu, C.K. Maurer, B. Kirsch, A. Steinbach, R.W. Hartmann, Overcoming the unexpected functional inversion of a PqsR antagonist in *Pseudomonas aeruginosa*: an *in vivo* potent antivirulence agent targeting pqs quorum sensing, Angew. Chem. Int. Ed. Engl. 53 (2014) 1109–1112, https://doi.org/10.1002/anie.201307547.